

This manuscript has undergone peer-review and has been accepted for publication in the journal Basin Research but has not undergone typesetting by the publisher. An updated peer-reviewed publication DOI link will be included to the right of this webpage when it becomes available



33 for the evolution of salt-related structures in rift basins with multiple stratigraphically discrete  
34 salt layers.

## 35 Highlights

- 36 • Upper Permian and Upper Triassic salt layers present in the Slyne and Erris basins.
- 37 • Zechstein Group forms salt pillows and reactive diapirs, Uilleann Halite forms  
38 reactive diapirs.
- 39 • Even thin salt layers act as prominent décollement surfaces during rifting.
- 40 • Stratigraphically discrete salt layers interact during structural evolution.

## 41 Acknowledgements

42 This research is funded in part by a research grant from Science Foundation Ireland (SFI)  
43 under Grant Number 13/RC/2092 and is co-funded under the European Regional  
44 Development Fund, and by the Petroleum Infrastructure Programme (PIP) and its member  
45 companies. Efstratios Delogkos is thanked for thoughtful discussions regarding the links  
46 between the Slyne and Erris basins and the Bróna and Pádraig basins. Neil Jones and Kristian  
47 Lomas are thanked for engaging discussions on the structural evolution of the Slyne and  
48 Goban Spur basins respectively. The authors would like to thank reviewers Torsten Hundebøl  
49 Hansen and Timothy Shin and associate editor Craig Magee for their constructive reviews  
50 which greatly improved the manuscript. The authors would like to thank the Petroleum Affairs  
51 Division (PAD) of the Department of Communications, Climate Action and Environment  
52 (DCCAE), Ireland, for providing access to released well, seismic, and potential field datasets.  
53 Europa Oil & Gas are thanked for providing access to the Inishkea 2018 reprocessed seismic  
54 volume and allowing a section from the volume to be shown. Shell Exploration & Production  
55 Ireland Ltd. are thanked for providing access to reprocessed volumes of the 1997 Corrib  
56 seismic. The authors would also like to thank Schlumberger for providing academic licenses  
57 of Petrel to University College Dublin.

## 58 Data Availability Statement

59 The data that support the findings of this study were provided by the Petroleum Affairs Division  
60 (PAD) and are available for download from [https://www.dccae.gov.ie/en-ie/natural-  
61 resources/topics/Oil-Gas-Exploration-Production/data/Pages/Data.aspx](https://www.dccae.gov.ie/en-ie/natural-resources/topics/Oil-Gas-Exploration-Production/data/Pages/Data.aspx). Restrictions may  
62 apply to the availability of these data, which were used under licence for this study.

## 63 1. Introduction:

64 Salt plays an important role in the development of sedimentary basins, acting as a layer of  
65 mechanical detachment between pre- and post-salt stratigraphy (Hudec & Jackson, 2007;  
66 Jackson & Hudec, 2017b). This leads to significant differences in the structural styles and  
67 evolution of salt-influenced basins relative to those unaffected by salt. Thick layers of salt have  
68 been encountered in several basins across the European Atlantic margin, including offshore  
69 Iberia (Wilson et al., 1989; Alves et al., 2006; Pena dos Reis et al., 2017; Ramos et al., 2017;  
70 Zamora et al., 2017), offshore France (Chapman, 1989; Ferrer et al., 2012), on the United  
71 Kingdom Continental Shelf (UKCS) (Stewart et al., 1996; Jackson & Stewart, 2017) and  
72 offshore Norway (Jackson et al., 2019; Rojo et al., 2019). Salt is also present in basins on the  
73 conjugate margin of Atlantic Canada (Jansa et al., 1980; Deptuck & Kendell, 2017). In these  
74 areas, the main layers of salt range in age from Early Permian to Early Jurassic, and have had  
75 a profound impact on basin development, commonly having undergone significant halokinesis  
76 to form distinctive salt-related structures such salt diapirs and allochthonous salt sheets and  
77 canopies (McKie, 2017; Stoker et al., 2017).

78 The Irish Atlantic margin has seen comparatively little research investigating the presence and  
79 impact of salt, owing to the limited well penetrations and lack of characteristic salt-related  
80 structures on seismic data. Nevertheless, Upper Triassic salt is proven in the Celtic Sea basins  
81 (Robinson et al., 1981; Van Hoorn, 1987; Shannon, 1991), the Central Irish Sea and St  
82 George's Channel basins (Naylor & Shannon, 1982) and the Kish Bank Basin (Naylor et al.,  
83 1993; Dunford et al., 2001). In the Porcupine Basin, Croker & Shannon (1987) reported the  
84 presence of salt in two wells in the north of the basin, while the 35/19-1 well encountered 24m  
85 of ?Upper Triassic allochthonous salt within Upper Jurassic sediments (Britoil, 1986; Merlin  
86 Energy Resources Consortium, 2020). Salt has also been identified onshore Ireland, within  
87 the Ulster-Larne Basin of Northern Ireland (Illing & Griffith, 1986; McCann, 1988; Quinn et al.,  
88 2010) and in a small outlier at Kingscourt, Co. Cavan (Gardiner & Visscher, 1971; Gardiner &  
89 McArdle, 1992). Previous work has noted the presence of salt in the Slyne and Erris basins  
90 (Tate & Dobson, 1989; Chapman et al., 1999; Dancer et al., 1999; Dancer et al., 2005) but  
91 limited and poor-quality seismic data, coupled with few well penetrations, made it difficult to  
92 assess the impact of these salt-prone layers on basin development. Since then, significantly  
93 more seismic data has been acquired and additional exploration wells have been drilled,  
94 allowing the nature of salt and the role it plays in the evolution of the Slyne and Erris basins  
95 to be investigated in greater detail (Fig. 1).

96 This study utilizes an extensive database of 2D and 3D multichannel seismic reflection data,  
97 coupled with wireline, cuttings and core data from exploration wells and shallow boreholes to

98 understand the distribution and composition of salt in the Slyne and Erris basins, and the  
99 impact of salt on the structural evolution of these basins. Both Upper Permian (Zechstein  
100 Group) and Upper Triassic (Uilleann Halite Member) salt layers have now been identified over  
101 significant parts of the study area. The Uilleann Halite Member was referred to as the Mercia  
102 Halite Member (e.g. Corcoran & Mecklenburgh, 2005; Dancer et al., 2005) prior to recent  
103 updates to the stratigraphic framework for offshore Ireland (Merlin Energy Resources  
104 Consortium, 2020). The occurrence of two salt layers results in stacked salt-related structures  
105 with evidence for interaction between halokinetic features developed at different structural  
106 levels.

107 In our study the distribution of salt on the Irish Atlantic margin is placed in regional context to  
108 provide insights into Late Permian and Late Triassic paleogeography of the north-western  
109 European Atlantic margin. The influence of salt on the petroleum systems of the Slyne and  
110 Erris basins is also discussed. The evolutionary model for halokinetic structures involving  
111 multiple thin salt layers may be applicable to other rift basins beyond the Irish Atlantic margin,  
112 particularly across NW Europe where several basins have multiple, stratigraphically discrete  
113 layers of salt.

## 114 2. Geological Setting:

115 The Slyne and Erris basins are contiguous rift basins located on the Irish Mainland Shelf off  
116 the north-western coast of Ireland in water depths of 150m to 3000m. They are narrow,  
117 elongate and broadly NE-SW oriented basins, which belong to a framework of rift basins  
118 extending westward from the coast of Ireland across the Irish Atlantic margin to the Atlantic  
119 Abyssal Plain. They form part of chain of rift basins stretching along the European Atlantic  
120 margin from the Barents Sea offshore northern Norway to offshore Portugal (Fig. 1). These  
121 rift basins formed during episodic extensional periods beginning with Variscan orogenic  
122 collapse and culminating with the onset of oceanic crust formation in the North Atlantic Ocean  
123 during the Eocene (Doré et al., 1999, Stoker et al., 2017; Schiffer et al., 2019).

### 124 2.1. Tectonostratigraphic evolution of the Slyne and Erris 125 basins:

126 The Slyne and Erris basins began to form during the Permian breakup of Pangea. Extension  
127 created a series of narrow, NE-SW and NNE-SSW oriented half-grabens (Fig. 1; Chapman et  
128 al., 1999; Dancer et al., 1999). The arid Permian climate led to the deposition of the Zechstein  
129 Supergroup, a large and widely studied 'salt giant' present across north-western Europe  
130 (Coward, 1995; Stewart, 2007; Duffy et al., 2013; Jackson & Stewart, 2017). This salt body  
131 formed through the ingress and subsequent evaporation of marine waters from the Boreal  
132 Ocean to the north (McKie, 2017). Possible pathways connecting the Irish Atlantic margin and  
133 the Boreal Ocean include the Faroe-Shetland Basin, the Hebridean basins, and an incipient  
134 Rockall rift system (Štolfová & Shannon, 2009; McKie & Shannon, 2011; McKie, 2017).  
135 Extension ceased by the Early Triassic, with thick fluvial and aeolian sandstones being  
136 deposited regionally, followed by the widespread deposition of playa-lake mudstones and  
137 siltstones and locally thick halite deposits during the Late Triassic (Štolfová & Shannon, 2009;  
138 Merlin Energy Resources Consortium, 2020).

139 The end of the Triassic was marked by a regional marine transgression and the deposition of  
140 shallow marine limestones, sandstones and mudstones during the Rhaetian to the Sinemurian  
141 (Trueblood & Morton, 1991; Raine et al., 2020). The area experienced mild extension during  
142 this time, with subtle syn-extensional thickening of the Lower Jurassic section occurring in the  
143 hanging-walls of active basin-bounding faults (Dancer et al., 1999). Intrabasinal NE-SW and  
144 NNE-SSW striking listric faults formed throughout the basin above small salt rollers and salt  
145 pillows. A minor break during the early Pliensbachian created a subtle unconformity, above

146 which Late Pliensbachian to Bajocian marine sandstones, limestones and mudstones were  
147 deposited.

148 A major unconformity separates the Lower and Middle Jurassic marine sediments from the  
149 overlying Upper Jurassic fluvio-estuarine sediments, with the unconformity locally incising  
150 deeply enough to place the Oxfordian above the Pliensbachian and Sinemurian on the basin  
151 margins. The main phase of rifting occurred during this time, with movement on basin-  
152 bounding faults creating accommodation space for the deposition of several kilometres of  
153 Upper Jurassic sediments (Merlin Energy Resources Consortium, 2020). The Upper Jurassic  
154 sediments consist of Oxfordian terrestrial, fluvial and estuarine sandstones and mudstones  
155 with associated coal horizons, which grade upwards into marine mudstones, limestones and  
156 sandstones, indicating a regional marine transgression occurred during the Kimmeridgian and  
157 Tithonian (Fig. 2).

158 Rifting in the Slyne and Erris basins ceased at the end of the Jurassic, with the area  
159 experiencing kilometre-scale uplift and erosion during the Early Cretaceous. As rifting  
160 occurred in the Rockall Basin to the west, the Erris Basin in particular was subject to severe  
161 rift-shoulder uplift, undergoing greater uplift along the western margin of the basin while thick  
162 Cretaceous sediments were deposited along the basin's eastern margin (Chapman et al.,  
163 1999; Walsh et al., 1999). Areas that were separated from the Rockall Basin by intervening  
164 basement highs, such as the Erris Ridge, did not experience the same extent of rift-shoulder  
165 uplift. The Slyne Basin remained a relative high throughout the Cretaceous, shielded from rift-  
166 related subsidence in the Rockall Basin by the Porcupine High, with only a thin veneer of  
167 Lower and Upper Cretaceous sediments deposited throughout the basin.

168 As rifting in the Rockall Basin ceased towards the end of the Cretaceous, the basin underwent  
169 thermal subsidence, with the western margins of the northern Slyne and the Erris basins that  
170 had been subject to rift-shoulder uplift now experiencing kilometre-scale subsidence. Post-rift  
171 tectonic activity continued throughout the Paleocene, Eocene and Early Miocene, expressed  
172 as subtle normal and reverse movement on faults throughout the basins, and in the formation  
173 of E-W oriented strike-slip faults, likely related to along-strike movement on major Caledonian  
174 crustal lineaments like the Great Glen and Fair Head-Clew Bay lineaments (Cooper et al,  
175 2012; Le Breton et al., 2013; Anderson et al., 2018). The development of the North Atlantic  
176 Igneous Province during the mid-Eocene had an impact on the Slyne and Erris basins, with  
177 the intrusion of several sills into the Mesozoic basin-fill and the extrusion of thick basaltic lavas  
178 of the Druid Formation (Jolley & Bell, 2002). These layered basalt flows are thickest on the  
179 western margin of the Southern Slyne Sub-basin, the Northern Slyne Sub-basin and in the



180 Northern Erris Sub-basin, where they degrade the quality of seismic data beneath these  
181 volcanic layers (Dancer & Pillar, 2001).

## 182 2.2. Structural Framework & Basin Morphology

183 The Irish Mainland Shelf separates the Slyne and Erris basins from the island of Ireland to the  
184 southeast, while the Rockall Basin bounds the Erris Basin along its north-western margin, with  
185 the Slyne and Porcupine highs bounding the Slyne Basin along its western margin (Fig. 1).  
186 The Erris Ridge is a NE-SW oriented, discontinuous basement high that separates the Rockall  
187 Basin from the Erris Basin and the northern Slyne Basin (Cunningham & Shannon, 1997). The  
188 Porcupine Basin is located to the southwest of the Slyne Basin and separated from it by a  
189 narrow basement horst.

190 The present-day morphology of the Slyne and Erris basins is largely controlled by their location  
191 on the Irish Continental Shelf and the development of the neighbouring Rockall Basin; the  
192 seabed above the Slyne Basin is topographically flat with no bathymetric expression, while  
193 the Erris Basin dips westwards along the shelf break into the Rockall Basin. This dip is more  
194 subtle in the Northern Erris Sub-basin, where the Erris Ridge is present, and more pronounced  
195 in the Southern Erris Sub-basin, beyond the extent of the Erris Ridge. The Erris Basin is  
196 transected by several present-day canyon systems that feed into the Rockall Basin from the  
197 Irish Mainland Shelf.

198 The Slyne and Erris basins are transected by several crustal-scale structural lineaments (Fig.  
199 1), representing suture zones and terrane boundaries separating Caledonian and Pre-  
200 Cambrian basement terranes that were accreted during the Grenville and Caledonian  
201 orogenies (Chew & Stillman, 2009). These structural lineaments trend NE-SW across onshore  
202 Ireland, rotating to trend E-W as they continue westwards into the offshore domain (Hutton &  
203 Alsop, 1996). Younger Mesozoic rift basins are segmented where they cross these Caledonian  
204 lineaments to form sub-basins that exhibit differences in structural style and geology and that  
205 are separated by structural complex transfer zones (Fig. 1; Trueblood, 1992; Dancer et al.,  
206 1999). The Slyne Basin can be subdivided into three distinct sub-basins, the Southern,  
207 Central, and Northern Slyne sub-basins. The offshore extension of the Fair Head-Clew Bay  
208 lineament separates the Southern and Central Slyne sub-basins, while the offshore extension  
209 of the Great Glen Fault Zone separates the Central and Northern Slyne sub-basins (Fig. 1;  
210 Dancer et al., 1999). The Erris Basin has previously been subdivided into three sub-basins  
211 based on the predominant dip of the faults in the Mesozoic section (e.g. Chapman et al., 1999);  
212 for the purposes of this study the Northern and Central Erris sub-basins of previous literature  
213 have been combined.

### 214 3. Dataset and Methodology:

215 This study utilises an extensive, multi-vintage seismic dataset covering the majority of the  
216 Slyne and Erris basins as well as extending into neighbouring regions (Fig. 3). The seismic  
217 database contains both 2D and 3D seismic reflection data. The 2D database consists of 25  
218 surveys, acquired between 1975 and 2014 that total over 49,000 km in line-length. The 3D  
219 database comprises 12 seismic surveys with a total area of over 6000 km<sup>2</sup>, although there is  
220 a significant area of overlap in the Northern Slyne Sub-basin. Most of the 3D surveys were  
221 acquired between 1997 and 2003, with the 1997 Corrib 3D (Dancer & Pillar, 2001)  
222 reprocessed in 2006, 2012 and 2018. Seismic quality in the Slyne and Erris basins varies from  
223 very poor to good and is dependent on the near-seabed geology. Extensive Eocene volcanics  
224 of the Druid Formation extruded during the formation of the North Atlantic Igneous Province,  
225 as well as exceptionally hard limestones of the Upper Cretaceous Chalk Group cause  
226 widespread imaging problems, principally multiple generation, energy scattering and signal  
227 attenuation (Dancer & Pillar, 2001). The volcanics are thickest in the Northern Slyne Sub-  
228 basin and the Southern Erris Sub-basin, as well as atop the Erris Ridge, while the Chalk Group  
229 is present throughout the Erris Basin and in the Northern Slyne Sub-basin. Seismic resolution  
230 varies across the study area due to different frequencies used by individual seismic surveys.  
231 In general, the vertical seismic resolution used for identifying salt layers varies between 10-20  
232 m near the seabed to 70-120 m at c. 5 km below the seabed (one-quarter wavelength sensu  
233 Brown, 2011). Seismic sections are presented in European polarity (Brown, 2001), where a  
234 positive downwards increase in acoustic impedance corresponds to a positive (red) reflection  
235 event and a decrease corresponds to a negative (blue) reflection event. All sections are  
236 vertically exaggerated by a factor of three. Ball-ends are used to highlight where a fault  
237 terminates within a certain stratigraphic package, while faults without ball-ends are truncated  
238 by a younger unconformity.

239 The seismic database was tied to released exploration and production wells and shallow  
240 boreholes across the study area. To date, two exploration wells have been drilled in the Erris  
241 Basin (19/5-1 and 12/13-1A), while eight exploration wells have been drilled in the Slyne Basin;  
242 these include the 18/20-1 Corrib gas discovery well, in addition to four near-field exploration  
243 wells in the Northern Slyne Sub-basin (19/8-1, 19/11-1A, 18/20-7, 18/25-2), with a further three  
244 exploration wells drilled in the Central Slyne Sub-basin (27/4-1, 27/5-1, 27/13-1). In addition  
245 to exploration wells, seven appraisal and production wells from the Corrib gas field are also  
246 incorporated into this study. The 27/13-1 well terminated in the Lower Jurassic, five other wells  
247 penetrated the Permian (12/13-1A, 19/5-1, 19/8-1, 18/25-2, and 27/5-1), with the remainder  
248 terminating in the Lower Triassic.

249 Exploration wells from neighbouring basins were also included to assess the distribution of  
250 salt beyond the boundaries of the Slyne and Erris basins; these include the 12/2-1z and 12/2-  
251 2 wells from the Rockall Basin, the 13/3-1 and 13/12-1 wells from the Donegal Basin, and the  
252 26/22-1A, 26/21-1, 26/30-1 and 35/19-1A wells from the Porcupine Basin. The well database  
253 is supplemented by three shallow boreholes; a single shallow borehole (11/20-sb01) drilled  
254 on the crest of the Erris Ridge (Haughton et al., 2005), and two shallow boreholes (19/13-sb01  
255 and 27/24-sb01) drilled in the Northern and Southern Slyne sub-basins respectively (Fugro,  
256 1994). Data from the deep exploration wells include full suites of wireline logs (caliper, gamma,  
257 density, neutron-porosity, resistivity, sonic), biostratigraphically-constrained formation tops,  
258 cuttings descriptions, core photos, and time-depth relationships in the form of checkshots or  
259 vertical seismic profiles (VSPs). The shallow borehole data include lithological descriptions,  
260 formation tops, core photos, and select geochemical and geotechnical samples.

261 Evaporites in both the Late Triassic and Late Permian sections were identified using a  
262 combination of wireline log data, cutting observations taken from both well completion reports  
263 and composite logs, and core data, where available. With the relatively limited well database  
264 available in the Slyne and Erris basins, the Permian and Late Triassic sections were sub-  
265 divided simply; the Permian section was divided into three categories based on the proportion  
266 of salt encountered, these being salt-dominated, transitional and clastic-dominated. Salt-  
267 dominated sections are composed overwhelmingly of salt lithologies such as halite and  
268 anhydrite, while clastic-dominated sections contain only sub-metre stringers of salt lithologies  
269 in a background of sandstones, mudstones and carbonates. The transitional category contains  
270 salt beds greater than a metre in thickness in a section largely composed of clastic and  
271 carbonate lithologies. Stratigraphic sub-division has already been established for the Late  
272 Triassic section, this being the presence or absence of the Uilleann Halite Member within the  
273 Currach Formation (Fig. 2).

274 Seismic reflection data were used to map the extent of salt beyond areas where it has been  
275 proven in borehole data. Halite mechanically detaches sub- and supra-salt sections, forming  
276 distinct décollement surfaces on seismic sections, and can form distinct structures including  
277 salt rollers, pillows and diapirs which can be used to indicate the presence of halite in the  
278 section of interest (*sensu* Hudec & Jackson, 2007). Detailed seismic interpretation throughout  
279 the Slyne and Erris basins alongside identification of salt-related structures therefore provided  
280 a framework for mapping the distribution of both Permian and Triassic salt intervals within the  
281 study area.

## 282 4. Salt Distribution and Composition:

283 Two layers of salt have been identified in the Slyne and Erris basins; the Zechstein Group,  
284 and the Uilleann Halite Member within the Currach Formation. As well penetrations are  
285 relatively limited in the Slyne and Erris basins, seismic character was used to constrain the  
286 composition of salt-prone intervals away from areas with well-control.

### 287 4.1. Zechstein Group

288 The Zechstein Group has been proven in all five exploration wells that penetrate the pre-  
289 Triassic section in the Slyne and Erris basins (12/13-1A, 19/5-1, 19/8-1, 18/25-2, 27/5-1), with  
290 variable lithologies encountered (Fig. 4). In the 12/13-1A in the Northern Erris Sub-basin, the  
291 Zechstein Group was largely composed of dolomite and anhydritic siltstones, with centimetre-  
292 scale stringers of anhydrite encountered throughout the section and reported from sidewall  
293 cores (Amoco, 1979). The Zechstein Group encountered in the 19/5-1 well in the Southern  
294 Erris Sub-basin and the 19/8-1 well in the Northern Slyne Sub-basin consisted of interbedded  
295 brown-red-grey mudstones and grey, microcrystalline dolomite accompanied by metre-scale  
296 stringers of anhydrite (Amoco, 1978; StatoilHydro, 2009). In the 18/25-2 well in the Northern  
297 Slyne Sub-basin, the Zechstein is composed of massive anhydrite alongside thin layers of  
298 microcrystalline dolomite and limestone at the top of the section, and thin layers of red-black  
299 mudstone towards the base of the sequence (Enterprise, 2000a). In the 27/5-1 well in the  
300 Central Slyne Sub-basin over 150 metres of massive halite was encountered, with thin  
301 magnesium salts encountered at the top of the section and interbedded anhydrite and  
302 claystone present towards the base of the section (Enterprise, 1996a). A 21-metre core was  
303 cut in the halite-prone section in the 27/5-1 well, described as white-pink-orange brittle halite  
304 (Fig. 4). These five well penetrations indicate a broad southward increase in the salt content  
305 of the Zechstein Group in the Slyne and Erris basins. Sediments belonging to the Zechstein  
306 Group may have been encountered at the base of some appraisal and production wells from  
307 the Corrib gas field; a mudstone-dominated section with minor anhydrite is present at the base  
308 of the Corrib Sandstone Formation in the 18/20-4 and 18/25-3 wells (Enterprise, 2000b, c).  
309 However, as these intervals are biostratigraphically barren (P. Copestake, pers. comm.) this  
310 remains unproven.

311 The variation in lithology of the Zechstein Group creates distinct wireline log profiles for both  
312 the salt-dominated and salt-poor forms. Salt-dominated sections have a characteristic blocky  
313 profile with low gamma ray values and high sonic velocities, while interbedded mudstone- and  
314 limestone-prone sections produces a more typical serrated wireline log character, higher  
315 gamma ray values and slower sonic velocities (Fig. 4).

316 When imaged on seismic data, the seismic response of the top Zechstein Group is often  
317 determined by the lithology at the base of the overlying Corrib Sandstone Formation. Where  
318 the Corrib Sandstone Formation is sandstone dominated towards the base, such as the  
319 Northern Slyne Sub-basin, a distinct negative impedance (blue) 'top-salt' reflector is observed  
320 (e.g. Fig. 5A, B). In areas where there is a greater proportion of mudstone and siltstone  
321 towards the base of the Corrib Sandstone Formation, such as the 27/5-1 well in the Central  
322 Slyne Sub-basin (Fig. 4), there is a less distinct 'top-salt' reflector (e.g. Fig. 6A). The unit itself  
323 is characterised by low-amplitude, bedded to chaotic reflectors, while local high-amplitude  
324 reflectors are occasionally observed and may represent clastic or carbonate bodies  
325 interbedded within halite-dominated areas (Fig. 7), although none of these high-amplitude  
326 bodies have been drilled to date. In areas of thinner, clastic-dominated Zechstein Group  
327 facies, the Permian section is often only represented by a single seismic wavelet (e.g. 19/5-1  
328 well and seismic wavelet comparison in Figure 4).

329 Well penetrations and seismic data suggest the proportion of salt within the Zechstein Group  
330 decreases northwards, with only sub-metre scale stringers of anhydrite present in the 12/13-  
331 1A well, the most northerly in the basin (Fig. 1, 4). Seismic data from the undrilled Southern  
332 Erris Sub-basin suggests the presence of a salt-prone Permian section, where a distinct  
333 detachment surface is observed beneath the Triassic section.

## 334 4.2. Currach Formation & Uilleann Halite Member

335 The Upper Triassic Currach Formation has been encountered in every well in the Slyne and  
336 Erris basins, except the 18/25-2 well where the Upper Triassic succession was faulted out.  
337 The formation consists predominantly of red mudstone, locally accompanied by minor  
338 siltstone, limestone, dolomite and anhydrite. Towards the base of the formation, a series of  
339 metre-scale halite beds is present. In the Northern Slyne and Southern Erris sub-basins, a  
340 halite-dominated section, termed the Uilleann Halite Member, is developed at the base of the  
341 Currach Formation. This comprises brittle, crystalline white to pinkish grey halite (Enterprise,  
342 1996b). The sediments of the Currach Formation reflect the arid lacustrine and sabkha  
343 conditions present in the Slyne and Erris basins during the Early Triassic, while the Uilleann  
344 Halite Member is indicative of a marine incursion into the Northern Slyne and Southern Erris  
345 sub-basins during the Middle to Late Triassic (Stoker et al., 2017).

346 The wireline log profiles of the Currach Formation consist of high gamma ray values and high  
347 sonic velocities associated with the mudstones that make up the bulk of the formation (Fig. 8).  
348 Interbedded siltstones, sandstones and carbonates typically have lower gamma ray values  
349 and slightly slower sonic velocities. The Uilleann Halite Member and smaller halite beds at the

350 base of the Currach Formation have very low gamma ray values and high sonic velocities,  
351 producing blocky wireline log profiles (Fig. 8). The Uilleann Halite Member is compositionally  
352 distinct from the Upper Permian salt, containing significantly more interbedded layers of red  
353 mudstone compared to the purer halite section in the Zechstein Group.

354 The top of the Currach Formation is marked by a high-amplitude soft or blue reflector on  
355 seismic data while the base of the formation is marked by a hard or red reflector representing  
356 the contact with the underlying Corrib Sandstone Formation (e.g. Fig. 5). The Currach  
357 Formation has a predominantly low-amplitude and chaotic seismic facies, with no clear  
358 distinction on seismic data with the Uilleann Halite Member. This is demonstrated in Figure  
359 5B where the Upper Triassic section in the 18/20-7 well is predominantly red mudstone with  
360 only 13 metres of halite present while the 18/20-3 and 18/20-6 wells drilled a halite section  
361 over 600 metres thick (Fig. 8) with little seismic variation between the two well locations.

362 While the Currach Formation has been proven in every well except 18/25-2 for reasons  
363 described above, well data suggest the Uilleann Halite Member is restricted to the Northern  
364 Slyne Sub-basin. The Uilleann Halite Member has been proven in the wells associated with  
365 the Corrib gas field (blocks 18/20 and 18/25) in addition to 18/20-7, 19/11-1A and 19/8-1. No  
366 salt is present in the Currach Formation in either the 12/13-1A or 19/5-1 wells on the margins  
367 of the Erris Basin, while only very minor stringers of anhydrite were encountered in the 27/5-  
368 1 and 27/4-1 wells in the Central Slyne Sub-basin. The 27/13-1 well terminated at the base of  
369 the Lower Jurassic section, while the 27/24-sb02 shallow borehole in the Southern Slyne Sub-  
370 basin encountered sub-metre beds of gypsum towards the base of the Currach Formation  
371 (Fugro, 1994). Seismic data from the Southern Erris Sub-basin suggests the Uilleann Halite  
372 Member extends northwards into this part of the basin, with two detachment surfaces visible;  
373 the lower detachment occurring on the salt of the Zechstein Group, while the upper  
374 detachment occurs within the Uilleann Halite Member.

### 375 4.3. Other salt-prone intervals in the Slyne & Erris basins

376 In addition to the Permian and Triassic salt present in the Slyne and Erris basins, several  
377 metres of anhydrite are interbedded with the sandstones, mudstones and limestones of the  
378 Lower Jurassic Meelagh Formation (Fig. 2). This anhydrite is developed in the Northern and  
379 Central Slyne sub-basins, with beds up to 20 metres thick encountered throughout the  
380 Meelagh Formation in the 18/20-1 well (Enterprise, 1996b), but thinning northwards, with no  
381 salt observed in the 19/11-1A well (Statoil, 2004). Only sub-metre-scale anhydrite stringers  
382 are recorded in the 19/8-1 well in the Northern Slyne Sub-basin, as well as the 19/5-1 and  
383 12/13-1A wells in the Erris Basin (Amoco, 1978; Amoco, 1979; StatoilHydro, 2009). The

384 Meelagh Formation was deposited in an arid climate (Merlin Energy Resources Consortium,  
385 2020), with the rapid vertical variation in facies representing an unstable and variable marginal  
386 marine to marine environment. Like the salt-prone intervals in the Zechstein Group and  
387 Uilleann Halite Member, the anhydrite beds within the Meelagh Formation have very low  
388 gamma-ray values and high sonic velocities on wireline logs. There is no evidence of  
389 mechanical detachment on the anhydrite beds of the Meelagh Formation seen on seismic  
390 sections from the Slyne and Erris basins, although it is possible that local, sub-seismic bed-  
391 parallel slip has occurred where these evaporites are present.

392 Within the Visean section of the 19/5-1 well in the Erris Basin, a sidewall core and cuttings at  
393 2141 metres Measured Depth (mMD) are described as claystones containing stringers of  
394 white anhydrite (Amoco, 1978). Gypsum has been encountered onshore Ireland in the  
395 equivalent section in the Lough Allen Basin (Ambassador, 1962; Grennan, 1992). While this  
396 section was only reached in a single well in the Erris Basin, it indicates the presence of salt-  
397 prone strata at four discrete stratigraphic levels (Carboniferous, Upper Permian, Upper  
398 Triassic, and Lower Jurassic) in the Slyne and Erris basins.

## 399 5. Salt structures in the Slyne and Erris basins

400 In areas of sparse well control, evidence of salt-related structures is supported by the  
401 identification of characteristic features on seismic data. The distribution and types of salt  
402 structures observed within the Slyne and Erris basins varies significantly between different  
403 sub-basins. This section analyses several of these structures and their implications for  
404 understanding salt composition and distribution.

### 405 5.1. Southern and Central Slyne Sub-basins

406 In the south of the study area only the Zechstein Group is salt prone, whereas the Uilleann  
407 Halite Member is not developed within the Currach Formation. In this area the Zechstein  
408 Group acts as a décollement between the pre-salt basement and the post-salt Mesozoic  
409 section. The Southern and Central Slyne sub-basins are two contiguous half-graben which dip  
410 steeply westwards towards the basin-bounding fault running along their western margins,  
411 across which they are downthrown relative to the Porcupine High. The Central Slyne Sub-  
412 basin is downthrown relative to the Southern Slyne Sub-basin across the offshore extension  
413 of the Highland Boundary-Fair Head Clew Bay Lineament (Fig. 1).

414 In the Southern Slyne Sub-basin, a single, relatively large salt roller is identified in the centre  
415 of the sub-basin (Fig. 7). The Triassic, Lower Jurassic and Middle Jurassic sections dip more  
416 steeply north-westwards than both the underlying Carboniferous basement and the overlying  
417 Upper Jurassic section, with the Base Upper Jurassic Unconformity eroding the crest of the  
418 structure.

419 In the Central Slyne Sub-basin there are several high-relief, broadly anticlinal structures in the  
420 immediate hanging-wall of the bounding fault along the western margin of the basin (Fig. 6).  
421 While ostensibly similar, each structure exhibits subtle variations in geometry and  
422 composition. The Triassic to Middle Jurassic section penetrated in the 27/4-1 well in the  
423 immediate hanging-wall of the bounding fault was encountered at similar depths in the 27/5-1  
424 well on the eastern margin of the Central Slyne Sub-basin (Fig. 6A). The Upper Jurassic  
425 section onlaps the steeply dipping eastern flank of the 27/4-1 structure, consistent with a  
426 predominately Late Jurassic age for the basin-bounding fault. The Upper Jurassic section also  
427 thickens eastwards into the hanging-wall of a major listric fault (Fig. 6A), indicating that  
428 movement on this fault occurred in tandem with the basin-bounding fault. The southern-most  
429 hanging-wall structure (Fig. 6B) is another high-relief anticlinal closure, with the Lower and  
430 Middle Jurassic section adjacent to the bounding-fault at a similar depth to the same section  
431 on the eastern margin of the basin. There is a distinct rotation of the Lower and Middle Jurassic



432 section facilitated by a detachment surface above the Triassic, suggesting the presence of  
433 halite within the Currach Formation at this location.

434 Between these two high-relief structures there is a relative saddle abutting the basin-bounding  
435 fault, forming a gently dipping dome. A distinct angular unconformity is observed beneath the  
436 Upper Jurassic section (Fig. 6C) which is not observed at the crests of the structures along-  
437 strike (Fig. 6A & B). Correlation from the 27/4-1 well indicates that the Middle Jurassic Kite  
438 Group and a significant portion of the Lower Jurassic Lias Group, down to the Pabay  
439 Formation, are absent from the crest of this saddle (Fig. 6C), while being preserved along-  
440 strike at the higher relief 27/4-1 location (Fig. 6A). This indicates that this location was at a  
441 higher relief relative to the present-day high-relief structures to the north and south during the  
442 period of uplift and erosion that preceded Oxfordian rifting. This elevated area was likely to  
443 have been cored by a gentle salt pillow before the emergence of the basin-bounding fault. As  
444 the main phase of rifting initiated during the Oxfordian, the structures to the north and south  
445 of this small salt pillow began to form, evidenced by onlap onto their flanks by the Upper  
446 Jurassic section in this part of the basin.

447 Similar to the structure shown in Fig. 6C, a significant section of the Middle and Lower Jurassic  
448 stratigraphy has been eroded from the eastern margin of the Central Slyne Sub-basin. The  
449 Kite Group and part of the Lias Group, down to the Pabay Formation, are absent beneath the  
450 base-Upper Jurassic unconformity in the 27/5-1 well while being present in the 27/4-1 well  
451 (Fig. 6A). The base-Upper Jurassic unconformity is encountered at a relatively similar depth  
452 present-day in both wells, 700 mMD and 845 mMD respectively (Merlin Energy Resources  
453 Consortium, 2020), while having significantly different subcrops, highlighting the variation in  
454 Zechstein Group salt topography during different extensional episodes.

455 The Central Slyne Sub-basin likely represents the erosional remnants of a significantly wider  
456 basin that included the Slyne Embayment and a smaller disconnected half-graben to the west  
457 of the Central Slyne Sub-basin (Fig. 1, 6A). The Slyne Embayment has a similar sedimentary  
458 fill to that of the Central Slyne Sub-basin, with the Triassic and Jurassic sections overlying a  
459 salt-prone Zechstein Group (Fig. 6A). Kilometre-scale erosion of the Jurassic section during  
460 the Cretaceous and Cenozoic (Dancer et al., 1999; Biancotto et al., 2007) is interpreted to  
461 have isolated the Slyne Embayment from the Central Slyne Sub-basin by eroding the footwall  
462 of the bounding fault along the western margin of the Central Slyne Sub-basin (Fig. 6A).

## 463 5.2. Northern Slyne Sub-basin

464 Several salt-cored folds are observed in the Northern Slyne Sub-basin, typically oriented NE-  
465 SW and NNE-SSW, parallel to the syn-rift faults. Composed of Zechstein salt, these pillows

466 are between 5 to 15 kilometres in length and up to 10 kilometres wide, often flanked by salt  
467 withdrawal synclines which likely developed by salt movement into the pillows (Fig. 5). The  
468 folded Mesozoic stratigraphy above these salt pillows has been the target of several  
469 exploration wells in this part of the basin, including the 18/20-1 (Corrib), 18/20-7 and 19/11-  
470 1A wells (Fig. 5B, C). Changes in the thickness of the Jurassic section in the flanking synclines  
471 indicate that the polarity of these salt pillows varied during basin evolution. The Lower and  
472 Middle Jurassic section in the syncline to the NW of the Corrib anticline is thicker than the  
473 syncline to the SE, while a thicker Upper Jurassic section is observed in the SE syncline  
474 relative to the NW (Fig. 5B).

475 Several of these salt-cored folds have large delamination faults above their crests which sole  
476 out into the Uilleann Halite Member at the base of the Currach Formation. These faults are  
477 parallel to the axes of the salt-cored folds and are likely to have developed in tandem with the  
478 pillows of Permian salt, representing outer-arc extension and gravitational collapse at the apex  
479 of the salt-cored folds. These delamination faults are often accompanied by the formation of  
480 salt rollers in their footwalls (Fig. 5A, B), in addition to faulted rollovers in their hanging-walls.

481 These delamination faults have been reactivated at several stages during the Cretaceous and  
482 Cenozoic post-rift period; significant growth sequences in the Cretaceous section are  
483 observed in the hanging-walls of these large delamination faults, particularly in the Lower  
484 Cretaceous Spurdog Formation (Fig. 5A, B). The delamination faults also offset the top of the  
485 Druid Formation lavas and a portion of the overlying Cenozoic sediments, which are dated as  
486 40-43 Ma in the 18/20-1 well (Dancer et al., 1999). The lack of folding in this Cretaceous and  
487 Cenozoic section indicates the later fault movement is more likely related to continued growth  
488 of the Upper Triassic salt roller rather than growth of the underlying Permian salt pillows and  
489 associated salt-cored folds.

### 490 5.3. Southern Erris Sub-basin

491 The Southern Erris Sub-basin dips steeply north-westwards as a result of post-rift thermal  
492 subsidence in the neighbouring Rockall Basin during the Cenozoic (Fig. 9-12). The western  
493 margin of the Erris Basin experienced significant rift-shoulder uplift during the Cretaceous,  
494 related to rifting in the Rockall Basin, with a kilometre-scale section of Jurassic stratigraphy  
495 removed. This part of the Erris Basin is dominated by a series of closely spaced (c. 1-2 km  
496 separation) westward-dipping faults in the Jurassic section (Fig. 9). Previous authors had  
497 interpreted these faults as through-going basement-linked structures (e.g. Shannon & Naylor,  
498 1998; Chapman et al., 1999; Corfield et al., 1999). However more recent seismic profiles  
499 reveal their listric nature, with many faults detaching on the Uilleann Halite Member above

500 closely spaced salt rollers (e.g. Fig. 9). The Zechstein Group also acted as a décollement in  
501 this part of the basin, mechanically detaching the Corrib Sandstone Formation from the  
502 underlying Carboniferous basement. Salt pillows formed in the Zechstein Group and folded  
503 the overlying Corrib Sandstone Formation in a similar manner to those in the Northern Slyne  
504 Sub-basin (Fig. 5)

505 More faults are through-going across the Permian section in the Southern Erris Sub-basin  
506 than in the Slyne Basin, suggesting that the Zechstein Group in this part of the basin may  
507 contain a greater proportion of clastic lithologies. The proportion of salt decreases towards the  
508 eastern margin of the Erris Basin, with faults being hard-linked through the Mesozoic and  
509 Palaeozoic sections (Fig. 10). Only a thin layer of anhydrite was encountered in the 19/5-1  
510 well drilled on the eastern edge of the Southern Erris Sub-basin (Fig. 4).

#### 511       5.4.     Northern Erris Sub-Basin

512 The Northern Erris Sub-basin is an asymmetric graben, bounded along its eastern margin by  
513 the Irish Mainland Shelf, and separated from the Rockall Basin to the west by the narrow,  
514 elongate Erris Ridge. The single well (12/13-1A) drilled in this part of the basin encountered  
515 only sub-metre-scale stringers of anhydrite in a 19 m thick Zechstein Group section, while no  
516 evaporite lithologies were present in the Currach or Meelagh formations. There is little  
517 evidence on seismic sections to indicate the presence of significant thicknesses of salt in this  
518 part of the basin, with all clearly imaged faults hard-linked through the Zechstein Group with  
519 little evidence for growth sequences in the pre-Triassic sections (Fig. 11, 12).

520 There is similarly scarce evidence for salt in neighbouring areas; both wells in the Donegal  
521 Basin to the northeast, 13/3-1 and 13/12-1 (Fig. 1), encountered the Pennsylvanian Blackthorn  
522 Group directly beneath the Base-Cenozoic Unconformity (Texaco, 1978; Lundin, 2006), while  
523 the 12/2-1 and 12/2-2 wells in the Rockall Basin to the west encountered the Triassic Cot  
524 Sandstone Formation (lateral equivalent to the Corrib Sandstone Formation) and Upper  
525 Jurassic Dawros Formation respectively lying directly above the Pennsylvanian Sorrel Group,  
526 with no Permian, Upper Triassic or Lower Jurassic sediment encountered (Merlin Energy  
527 Resources Consortium, 2020).

## 528 6. Discussion:

### 529 6.1. Timing and drivers of halokinesis in the Slyne and 530 Erris basins

531 Understanding the timing of salt movement during basin development is important both for  
532 unravelling the structural evolution and for understanding the development of the petroleum  
533 system. There is evidence of halokinesis occurring at several stages during basin evolution,  
534 including during both the Early to Middle Jurassic and Late Jurassic phases of rifting, in  
535 addition to post-rift modification of salt structures during the Cretaceous and Cenozoic.

536 In the Southern Slyne Sub-basin, the Triassic and Lower Jurassic section tilted above the  
537 large Zechstein Group salt roller is truncated by the Base Upper Jurassic unconformity (Fig.  
538 7). This suggests that inflation of the salt roller in the footwall of the fault began forming during  
539 the Early-Middle Jurassic before the crest was eroded, resulting in the angular unconformity,  
540 followed by further inflation during Late Jurassic rifting (Fig. 13). In the Central Slyne Sub-  
541 basin growth sequences are observed in the Lower Jurassic section in the hanging walls of  
542 small intra-basinal listric faults which sole out in the Upper Permian Zechstein Group (Fig. 6).  
543 The faults controlling these growth sequences are then truncated by the Base Upper Jurassic  
544 Unconformity, indicating discrete extension confined to the Early-Middle Jurassic. There is  
545 further evidence of Early Jurassic halokinesis in the Northern Slyne Sub-basin with subtle  
546 thinning of the Lower Jurassic section onto the crest of the Corrib anticline (Fig. 5B), indicating  
547 that the Zechstein Group salt pillow was creating relief during the Early Jurassic (Fig. 13).  
548 Faults of a similar age are also interpreted in the Southern Erris Sub-basin, where faults which  
549 sole out above rollers of Uilleann Halite are truncated by the Base Upper Jurassic  
550 Unconformity. Several of these faults have hanging-wall sequences that record limited growth  
551 during the Early Jurassic (Fig. 9) and were reactivated during the main phase of rifting during  
552 the Late Jurassic and subsequently truncated by the Base-Cretaceous Unconformity.

553 The main phase of rifting in the Slyne and Erris basins, during the Late Jurassic, was preceded  
554 by the formation of the regional Base Upper Jurassic Unconformity mentioned previously (Fig.  
555 13). The majority of intra-basinal faulting during this time occurred as thin-skinned, basement-  
556 detached deformation (Figs 5-7, 9) apart from in the Northern Erris Sub-basin where the  
557 Uilleann Halite Member is absent and the Zechstein Group is composed of carbonates and  
558 clastics (Fig. 11 & 12). In the Central Slyne Sub-basin growth sequences (Fig. 6A) and onlap  
559 (Fig. 6B) are observed on the flanks of the high-relief structures in the immediate hanging-wall  
560 of the basin-bounding fault. Unlike other high-relief structures where distinct crestal erosion is

561 recorded at the Base Upper Jurassic Unconformity, these structures likely emerged during  
562 Late Jurassic basin extension (Fig. 13). Their geometry, as well as the likely presence of salt  
563 in the Slyne Embayment to the west, indicate that these structures may have formed as forced  
564 folds above the active footwall of the basin-bounding fault, creating the topography for onlap  
565 and growth sequences (e.g. Withjack & Callaway, 2000; Coleman et al., 2017). The  
566 interpretation of salt in the undrilled Slyne Embayment to the west of the Central Slyne Sub-  
567 basin (Fig. 6A), further supports the idea that Permian salt and the overlying Mesozoic section  
568 may have overstepped the now eroded footwall of the bounding fault before kilometre-scale  
569 uplift and erosion during the Cretaceous and Cenozoic (Fig. 6A).

570 Along-strike variation in the anticlinal structures adjacent to the bounding fault in the Central  
571 Slyne Sub-basin suggests there may be more complexity to their evolution beyond a breached  
572 salt-detached monocline. Dancer et al. (1999) suggested five potential mechanisms for the  
573 formation of the structure targeted by the 27/4-1 well (Fig. 6A), with one being salt diapirism.  
574 Crucially, that paper predated the acquisition of good-quality 3D seismic data (2000) and the  
575 drilling of the 27/4-1 well (2009), datasets which highlight the modification of these structures  
576 during basin evolution. Specifically, the preservation of the Middle and Lower Jurassic section  
577 proven in the 27/4-1 well, combined with the absence of the Kite Group and Dun Caan Shale  
578 and Whitby Mudstone formations along-strike (Fig. 6C), highlights the modification of  
579 structures during basin evolution, with the eroded crest of the structure in Fig. 6C being over  
580 600ms TWT (c. 1200m) deeper than the seemingly uneroded crest of the structure in Fig. 6A.  
581 This evidence suggests there may have been a high-relief salt-cored structure during the Early  
582 and Middle Jurassic at the location of Fig. 6C, possibly a salt pillow or a large salt roller similar  
583 to that imaged in Fig. 7 which exhibits comparable crestal erosion. This salt pillow or salt roller  
584 collapsed during the Late Jurassic rifting with along-strike migration of the Permian salt into  
585 the present-day higher elevation structures. As the apparent volume of salt present between  
586 these anticlinal closures and the basin-bounding fault is relatively small, salt may also have  
587 been extruded into salt diapirs on the now eroded footwall of the basin bounding fault.

588 Several salt structures in the Slyne Basin underwent significant post-rift modification during  
589 the Cretaceous and Cenozoic, driven by rifting in the Rockall Basin during the Cretaceous,  
590 and subsequent Cenozoic post-rift thermal subsidence, mid-Atlantic ridge-push and the  
591 development of the Icelandic plume (Dancer et al., 1999). There is evidence throughout the  
592 Slyne and Erris basins of fault reactivation, with several of these reactivations occurring in  
593 salt-prone areas where the faults are listric and sole out in either the Zechstein Group or the  
594 Uilleann Halite Member (Fig. 6 & 9). Other structures appear not to have been reactivated  
595 during this post-rift activity (e.g. Fig. 7), although the lack of Cretaceous sediments in the  
596 Central and Southern Slyne Sub-basins means that any fault movement during this phase of

597 post-rift deformation is not recorded. This Cretaceous and Cenozoic reactivation is subtle, with  
598 movement on reactivated faults being in the order of 10s of metres, much lower than the syn-  
599 rift fault offsets which are in the order of several hundred metres to kilometres in scale.

600 Regional extension is recognised as a common mechanism for the initiation of salt tectonics  
601 (Jackson & Vendeville, 1994; Jackson & Hudec, 2017b) and is the most likely trigger for  
602 halokinesis in the Slyne and Erris basins. The seismic data analysed above indicates that  
603 there were two main phases of syn-rift halokinesis in the Slyne and Erris basins; the first of  
604 these occurred during Early to Middle Jurassic extension with a subsequent phase of salt  
605 movement during Late Jurassic rifting. Some salt structures formed during the first phase of  
606 halokinesis were reactivated and continued to grow during the Late Jurassic period of salt  
607 movement (e.g. Fig. 5-7), while others collapsed during this second phase of rifting (e.g. Fig.  
608 6C). It is also possible that other structures such salt diapirs formed above the footwalls of  
609 active faults due to extrusion of salt from collapsed structures which were subsequently eroded  
610 during Cretaceous uplift. Several salt-related structures underwent minor modification during  
611 post-rift tectonic activity in the Cretaceous and Cenozoic.

## 612 6.2. Kinematic interaction between salt layers

613 In the Northern Slyne and Southern Erris sub-basins, two distinct layers of autochthonous salt  
614 are present at different stratigraphic intervals, which has previously been termed 'double-  
615 decker' salt tectonics (Corcoran & Mecklenburgh, 2005). In these areas a clear relationship  
616 between the timing of halokinesis in each layer can be observed. The most well imaged of  
617 these is the structure containing the Corrib gas field, where two discrete salt-related structures  
618 are visible: a Zechstein Group salt pillow and an Uilleann Halite Member salt wall (Fig. 5B).  
619 These structures have parallel trends, oriented NE-SW (Fig. 5D). The Uilleann Halite diapir  
620 has a distinct pointed crest, indicating it is likely to be a reactive diapir which formed during  
621 delamination faulting of the Jurassic overburden. As the Zechstein salt pillow grew and folded  
622 the overlying Triassic and Jurassic section, outer-arc extension triggered listric delamination  
623 faulting in the Jurassic section at the crest of the fold, with these faults soling out in the Uilleann  
624 Halite (Fig. 13). The throw on these delamination faults is greatest at the apex of the Zechstein  
625 salt pillow and resultant Lower Triassic fold, where outer-arc extension facilitates the inflation  
626 of an Uilleann Halite salt roller (Fig. 5A) or in the case of the Corrib structure, a reactive diapir  
627 oriented parallel to the fold axis of the salt pillow (Fig. 5B, D).

628 While the Zechstein salt pillow controlled the initial evolution of the Uilleann Halite diapir, the  
629 subsequent growth of this diapir during continued extension may have in turn influenced the  
630 development of the salt pillow. As regional extension continued during the Late Jurassic, the

631 delamination fault above the Corrib anticline experienced further normal movement. This fault  
632 movement displaced the overburden section downwards off the crest of the anticline, creating  
633 thicker sedimentary sections in the flanking synclines (Fig. 5B) while reducing the sediment  
634 thickness at the apex of the fold. These thicker sedimentary sections on the flanks of the  
635 anticline are suggested to have inflated the Zechstein salt pillow further through differential  
636 loading, creating a steeper structure which would then lead to further movement on the crestal  
637 delamination fault. The delamination fault above the Corrib gas field was reactivated again  
638 during the Cretaceous and the Cenozoic, with distinct growth sequences observed in the  
639 Cretaceous section in the immediate hanging-wall of the delamination fault (Fig. 5B), which  
640 also offsets the top of the Druid Formation volcanics. This volcanic sequence is dated between  
641 54.3 and 40 Ma (early-mid Eocene) in the 18/20-1 well and the 19/13-sb02 shallow borehole  
642 in the Northern Slyne Sub-basin (Fugro, 1994; Corcoran & Mecklenburgh, 2005), indicating  
643 how recently this Permian-Triassic salt relationship was active. A similar relationship likely  
644 drove the syn- and post-rift evolution of other salt pillow and diapir pairs observed in the  
645 Northern Slyne and Southern Erris sub-basins (e.g. Fig. 5A, 9).

646 Previous structural models for the Corrib structure (e.g. Corcoran & Mecklenburgh, 2005;  
647 Dancer et al., 2005) have suggested a polarity reversal in the delamination fault at different  
648 stages of basin evolution, with an initial westward-dipping fault plane during the Early Jurassic  
649 changing to the dominant eastward-dipping fault observed today during the Late Jurassic. A  
650 thinner Lower and Middle Jurassic section encountered on the eastern flank of the anticline  
651 was interpreted as the eroded footwall of the westward-dipping fault relative to the thicker  
652 section observed on the western flank (Fig. 5B). Recent biostratigraphic analysis has revealed  
653 that complete Lias Group and Kite Group sections have been encountered in all wells drilled  
654 in the Corrib gas field, with an attenuated but complete section encountered in the Lower and  
655 Middle Jurassic on the eastern flank of the anticline (Merlin Energy Resources Consortium,  
656 2020). This attenuated section was likely deposited on the crest of a salt-cored fold during the  
657 Early and Middle Jurassic and is commonly observed above salt pillows (Jackson & Hudec,  
658 2017a). Significant heave on the delamination fault during the Late Jurassic moved the  
659 attenuated crestal section of Lower and Middle Jurassic sediments eastwards down the flank  
660 of the anticline. It is therefore more likely that the delamination fault above the Corrib salt-  
661 cored fold is a largely Late Jurassic structure which downthrows to the southeast. The polarity  
662 reversal of faults above salt walls is a common feature of mature halokinetic structures (e.g.  
663 Quirk & Pilcher, 2012) but due to the relative immaturity of the Upper Triassic salt wall a  
664 simpler structural model prevails. Polarity reversal is observed in thickness variations in the  
665 synclines flanking the Corrib anticline, with thicker Lower and Middle Jurassic section in the  
666 NW syncline and a thicker Upper Jurassic section in the SE syncline. This reversal is likely a

667 result of the emergence of the kilometre-scale faults bounding the eastern margin of the  
668 Northern Slyne Sub-basin during the Late Jurassic.

669 The kinematic interaction of stratigraphically discrete salt layers observed in the Slyne and  
670 Erris basins may act as a structural template for other basins which have multiple thin layers  
671 of salt (Fig. 13). Examples include the Sole Pit Basin and Danish Central Graben in the North  
672 Sea, where delamination faults sole out in the Triassic Muschelkalk Halite above folds cored  
673 by Zechstein Group salt (Glennie, 1997; Hansen et al., 2020).

### 674 6.3. Relationship between timing of halokinesis and the 675 petroleum system

676 The timing of formation and subsequent modification of the Corrib structure played a crucial  
677 role in both the success and failure of the 18/20-1 discovery well. The well was drilled to the  
678 northwest of the main delamination fault, passing through the tilted fault block above the  
679 Uilleann Halite diapir (Fig. 5B, D). The well encountered oil-stained sandstones throughout  
680 the Upper Jurassic section, evidence of a breached paleo-accumulation, before discovering  
681 the gas accumulation in the Corrib Sandstone Formation, sealed by the Uilleann Halite  
682 Member (Enterprise, 1996b; Dancer et al., 2005). Geochemical fingerprinting of these  
683 hydrocarbon fluids indicates that the oil is sourced from the Lower Jurassic Whitby Mudstone,  
684 Pabay Shale and Dun Caan Shale formations while the gas is presumed to be generated by  
685 coal layers in the Carboniferous basement (Dancer et al., 1999; Scotchman et al., 2018). Post-  
686 rift movement on the main delamination fault bounding the Jurassic structural trap (Fig. 5D)  
687 during both the Cretaceous (Fig. 5D) and Cenozoic (Fig. 5B) post-dates the main phase of  
688 hydrocarbon generation and migration at the end of the Jurassic (Petroleum Affairs Division,  
689 2005). This late movement on the delamination fault likely caused cross-fault juxtaposition of  
690 Upper Jurassic sandstones, possible dilation of the fault plane and breaching of the top seal,  
691 leading to the loss of the oil accumulation. However, since the delamination fault soles out in  
692 the Uilleann Halite Member, this post-charge fault movement did not interact with the Corrib  
693 Sandstone Formation and the gas accumulation.

694 Similarly, post-rift modification of the underlying Zechstein Group salt pillow may explain the  
695 nature of the Corrib anticlinal trap. The anticline is significantly underfilled, with potential  
696 associated mechanisms including the presence of a small leaking fault at the current gas-  
697 water contact or leakage through the sealing Uilleann Halite Member during Cretaceous and  
698 Cenozoic exhumation (Corcoran & Doré, 2002; Corcoran & Mecklenburgh, 2005). The modest  
699 overpressure within the reservoir section (Corcoran & Doré, 2002) and halite composition of  
700 the top-seal indicate that the original charge pre-dating exhumation is preserved and that



701 leakage without clear evidence of salt-welding is difficult. Salt tectonics may instead be  
702 responsible for the underfilled nature of the Corrib anticline, with post-rift movement on the  
703 delamination fault and growth of the Uilleann Halite Member diapir perhaps driven by post-rift  
704 growth of the Zechstein Group salt pillow. Additional post-rift (and post-charge) growth of this  
705 salt pillow would have increased the vertical relief of the anticline and its trap capacity. The  
706 volume of the structural trap from the Late Cretaceous onwards would therefore be larger than  
707 the volume of gas trapped during the Late Jurassic and Early Cretaceous, resulting in its  
708 underfilled nature observed at present. This highlights the multiphase evolution of this and  
709 probably other structures within the Slyne and Erris basins and illustrates how understanding  
710 their structural history will be critical to improving exploration success in the future.

## 711 6.4. The Slyne and Erris basins in context with other salt- 712 prone basins of the North Atlantic

713 Results presented thus far have highlighted the importance of salt during the structural  
714 evolution of the Slyne and Erris basins and defined a range of structures that are characteristic  
715 of salt-involved deformation in this area. By applying a similar methodology to that  
716 demonstrated above, we can delimit the occurrence of salt in neighbouring basins where the  
717 lack of well data has made interpretation of salt more speculative. A more detailed  
718 understanding of salt distribution can in turn be used to refine paleogeographic models for the  
719 Late Permian and Late Triassic of the Irish Atlantic margin.

### 720 6.4.1. Irish Atlantic Margin

721 No Permian rocks have been encountered outside of the Slyne and Erris basins on the Irish  
722 Atlantic margin to date, although Permian ages have been suggested for a sandstone section  
723 encountered above the Carboniferous in the 12/2-1 and 12/2-2 wells on the eastern margin of  
724 the Rockall Basin, adjacent to the northern Erris Basin (Shell, 2009; Tyrrell et al., 2010).  
725 Conversely, Early and Late Triassic-aged sections have been proven in several basins,  
726 including the Porcupine and Celtic Sea basins.

727 In the North Porcupine Basin metre-scale anhydrite layers were encountered towards the top  
728 of the Currach Formation in well 26/22-1A (BP, 1979), while the 35/19-1A well encountered  
729 24m of allochthonous salt in Upper Jurassic sediments on the eastern margin of the Porcupine  
730 Basin (Britoil, 1986). In this well the salt is composed of massive halite with thin slivers of red  
731 mudstone likely representing rafted sections of Currach Formation mudstones, suggestive of  
732 Upper Triassic salt, equivalent to the Uilleann Halite Member in the Slyne and Erris basins. As  
733 an Uilleann Halite Member equivalent has not been encountered in the northern Porcupine  
734 Basin to date, this Triassic salt is likely to have migrated from a more central, undrilled part of  
735 the basin to the south.

736 The Goban Spur Basin, along the southern margin of the Porcupine Basin (Fig. 1), may also  
737 contain Triassic salt, with evidence on seismic data of décollement surfaces and salt pillows  
738 beneath the Base-Cretaceous Unconformity (Fig. 14). A pronounced fold occurring above  
739 near-horizontal, unfolded reflectors (Fig. 14) is interpreted as local Lower Triassic sediments  
740 deposited within the Variscan fold and thrust belt but since the single well drilled in the Goban  
741 Spur Basin terminated in Lower Jurassic sediments, this interpretation remains speculation  
742 (Colin et al., 1992).

743 Previous authors have noted décollement surfaces in the perched basins along the margins  
744 of the Irish sector of the Rockall Basin, including the Bróna and Fursa basins on the eastern  
745 margin (Thomson & McWilliam, 2001; Štolfova & Shannon, 2009) and the Conall and Rónán  
746 basins on the north-western margin (Corfield et al., 1999; Walsh et al., 1999). Distinct  
747 detachment horizons are visible on seismic data from these basins, with faults observed soling  
748 out in these horizons. In the Rónán Basin on the western margin of the Rockall Basin, a subtle  
749 décollement is visible within the steeply dipping reflectors, mechanically detaching faults  
750 above and below it, with a distinct local thickening along the south-eastern margin of the basin  
751 interpreted as a salt pillow (Fig. 15A). Similarly, two distinct sets of faults are observed either  
752 side of a décollement in the Fursa Basin (Fig. 15B). While these basins are undrilled at  
753 present, these décollement surfaces likely represent lateral equivalents to Permian salt proven  
754 in the Slyne Basin, as interpreted by Štolfova & Shannon (2009). In these basins this layer of  
755 salt plays a similar role in mechanically detaching the Mesozoic basin fill, which displays  
756 similar seismic facies to those observed in the Slyne and Erris basins, from the Palaeozoic  
757 basement.

## 758           6.4.2.       Neighbouring basins on the European Atlantic 759                       margin

760 The basins of the Irish Atlantic margin belong to a chain of basins that extend along the  
761 European Atlantic margin, many of which also contain significant salt deposits that correlate  
762 with those proven in the Slyne and Erris basins. Directly north of the study area, a series of  
763 interconnected basins off the north-western coast of the UK contain significant thicknesses of  
764 sediments defined broadly as Permo-Triassic due to the relative lack of biostratigraphic control  
765 (Steel & Wilson, 1975; Hitchen et al., 1995). Both wells drilled in the West Orkney Basin  
766 encountered several hundred metres of halite interbedded with sandstones and mudstones  
767 with anhydrite stringers belonging to the West Orkney Evaporite Formation interpreted as  
768 being Permian in age and representing Zechstein Group equivalents (Elf, 1991; Hitchen et al.,  
769 1995; McKie, 2017). Along-strike in the West Shetland Basin the 205/27a-1 well encountered  
770 interbedded Upper Permian sandstones and mudstones with anhydrite stringers (Hitchen et  
771 al., 1995). There is little evidence of salt in the Upper Triassic section in this region, instead  
772 being dominated by sandstone (Swiecicki *et al.* 1995).

773

### 6.4.3. Implications for the Permian & Triassic

774

#### paleogeography of the Irish Atlantic margin

775

Paleogeographic reconstructions of north-western Europe during the Permian and Triassic often present the Irish Atlantic margin in simplified terms at the fringes of regional maps, owing to the relative lack of well penetrations and published data when compared with neighbouring regions. The Early Triassic is an exception, due to its significance in the petroleum system of the Corrib gas field (Dancer et al., 2005), with a relatively well understood paleogeography in which the Slyne and Erris basins are host to southwards-verging braided fluvial systems (e.g. Tyrell et al., 2007; McKie & Williams, 2009; Franklin et al., 2019). No Early Permian rocks have been encountered on the Irish Atlantic margin to date. Existing paleogeographic reconstructions (e.g. Doré, 1991; Knott et al., 1993; McKie & Shannon, 2011; McKie, 2017; Scotese & Schettino, 2017) present the Irish Atlantic margin as the terminus of tortuous seaways that extended into the Pangean supercontinent; During the Late Permian ingress of marine waters came from the Boreal Ocean to the north through the West of Shetland region, but during the Late Triassic a seaway extended from the Tethys Ocean to the southeast across Central and Western Europe to reach Ireland through the Cheshire Basin in the UK. Using the results presented in this study as well as the speculative interpretations of neighbouring regions discussed above, it is possible to refine existing paleogeographic models of the region during the Late Permian and Late Triassic, and include the basin-specific detail for the Irish Atlantic margin that was absent in previous regional syntheses.

793

The distribution of Late Permian salt of both the UK and Norwegian North Sea has been interpreted to be fault controlled, with salt-prone lithologies deposited in the hanging walls of active faults, while marginal carbonate and siliciclastic facies accumulated on basin margins and intra-basinal highs. The exact age of faulting remains ambiguous, with the Late Permian bathymetry either being inherited from Early Permian rifting, or representing syn-depositional extension in the Late Permian (e.g. McKie & Shannon, 2011; Jackson & Lewis, 2016; Jackson et al., 2019). Applying a similar model to the Slyne and Erris basins, the thicker salt-prone Zechstein Group in the Slyne Basin and the Southern Erris Sub-basin would be indicative of active Permian faulting, while the presence of thin marginal deposits in the Northern Erris Sub-basin suggests this area was a relative high with little active faulting. Therefore, the marine pathway connecting the Slyne Basin to the Boreal Ocean likely traversed an area other than the Erris Basin, an interpretation supported by the lack of Permian sediments in the north-eastern Irish Rockall Basin, the Donegal Basin and the Sea of the Hebrides Basin. The layers of salt interpreted in the Rónán Basin, the pre-Cretaceous 'conjugate margin' to the Erris Basin (Fig. 15A), might therefore indicate that the route of active Permian rifting may have been an

807

808 anastomosing series of rifts extending northwards along the axis of a proto-Rockall and West  
809 of Shetland rift system, with remnants of these basins occupying the margins of the Rockall  
810 Basin after rifting and hyperextension in the Cretaceous (Fig. 16A). This may indicate that the  
811 framework for the present-day configuration of rift basins on the Irish Atlantic margin may have  
812 been established in-part during this period of Permian extension.

813 During the Late Triassic, the Northern Slyne and Southern Erris sub-basins may have also  
814 been the terminus for a seaway, this time stretching from the Tethys Ocean to the southwest.  
815 The Uilleann Halite Member in the Northern Slyne and Southern Erris sub-basins (Fig. 1, 8)  
816 likely represents the deposits of incursions of marine brines from the southwest. In  
817 neighbouring regions such as the Ulster Basin and the Irish Sea basins several discrete layers  
818 of halite are interpreted as successive marine flooding events into these regions (Jackson &  
819 Mulholland, 1993; Dunford et al., 2001; McKie, 2017). The Uilleann Halite Member might  
820 therefore represent the deposits of a more extensive marine incursion that extended beyond  
821 those found in the Irish Sea and North Channel region. The exact route of marine ingress is  
822 uncertain and likely obscured by Cretaceous and Cenozoic erosion, but may have come from  
823 the south, through the Celtic Sea and Porcupine basins (e.g. Scotese & Schettino, 2017), or  
824 from the north or east through the Donegal Basin or the Ulster-Larne Basin (e.g. Naylor, 1992).  
825 The paleogeography of the Late Triassic salt layers is distinct from the Late Permian as these  
826 marine incursions flood a predominantly arid lacustrine environment, represented by the thick  
827 red mudstones which dominate the majority of the Currach Formation (Fig. 8), which differs  
828 from the predominantly marine environment of the Zechstein Group deposits, represented by  
829 cleaner halite with few mudstone inclusions (Fig. 4). Additionally, the Triassic was a period of  
830 tectonic quiescence on the Irish Atlantic margin following Permian rifting (e.g. Tyrrell et al.,  
831 2007; Franklin et al., 2019) and Late Triassic sediments likely spilled out beyond the present-  
832 day basin boundaries (Fig. 16B), with their present-day distribution a product of preservation  
833 in post-Triassic rift basins.

## 834 7. Conclusions

835 Using a combination of 2D and 3D seismic, wireline, and core data, this study investigated the  
836 distribution of the salt in the Slyne and Erris basins and its influence on the structural evolution  
837 of these basins.

- 838 1. Two main salt-prone intervals are present in the Slyne and Erris basins. The Upper  
839 Permian Zechstein Group is salt prone throughout the Slyne Basin and in the Southern  
840 Erris Sub-basin, becoming dominated by carbonates and clastics in the Northern Erris  
841 Sub-basin. The Upper Triassic Uilleann Halite Member is developed in the Northern  
842 Slyne Basin and Southern Erris sub-basins.
- 843 2. Salt acts as a décollement and mechanically detaches distinct sections of stratigraphy  
844 within the Slyne and Erris basins. The Zechstein Group has the largest impact on basin  
845 development and is a regional décollement surface, with most syn-rift normal faults  
846 detached from the pre-Permian basement along this surface. The Uilleann Halite  
847 Member exerts similar controls on basin development where it is present.
- 848 3. Halokinesis occurred at several stages during the evolution of the Slyne and Erris  
849 basins. This includes extension in the Early Jurassic and the Late Jurassic, as well as  
850 post-rift reactivation during the Cretaceous and Cenozoic. This salt movement has  
851 created a variety of relatively immature salt-related structures throughout the Slyne  
852 and Erris basins, including salt pillows, rollers and reactive diapirs.
- 853 4. Where both salt successions are developed, the topography created by the Zechstein  
854 Group halokinesis influences the development of salt-related structures in the  
855 overlying Uilleann Halite Member, exemplified in the parallel salt pillow and salt wall  
856 pair observed in the Corrib structure. Outer-arc extension and gravitational collapse  
857 linked with the formation of the Zechstein Group salt pillows leads to the formation of  
858 Uilleann Halite salt rollers and walls. This kinematic interaction may serve as a  
859 framework for the structural evolution of similar structures in other basins with multiple  
860 stratigraphically discrete layers of salt.
- 861 5. An improved understanding of the distribution and composition of Permian and Triassic  
862 salt in the Slyne and Erris basins and in undrilled basins along the Irish Atlantic margin  
863 indicates that the framework of sedimentary basins along the Irish Atlantic margin may  
864 have been established as early as the Late Permian.

## 865 References

- 866 Alves, T.M., Moita, C., Sandnes, F., Cunha, T., Monteiro, J.H. & Pinheiro, L.M. 2006.  
867 Mesozoic-Cenozoic evolution of North Atlantic continental-slope basins: The Peniche  
868 basin, western Iberian margin. *AAPG Bulletin*, **90**, 31–60.
- 869 Ambassador 1962. Dowra No. 1 Well Report. Ambassador Irish Oil Company.
- 870 Amoco 1978. Well 19/5-1 Geological Completion Report. Amoco Ireland Exploration  
871 Company, compiled by Odell, R.T. & Thomas, I.W.
- 872 Amoco 1979. Wells 12/13-1 and 12/13-1A Geological Completion Report. Amoco Ireland  
873 Exploration Company, compiled by Odell, R.T. & Walker, D.
- 874 Anderson, H., Walsh, J.J. & Cooper, M.R. 2018. The development of a regional-scale  
875 intraplate strike-slip fault system; Alpine deformation in the north of Ireland. *Journal of*  
876 *Structural Geology*, **116**, 47–63.
- 877 Biancotto, F., Hardy, R.J.J., Jones, S.M., Brennan, D. & White, N.J. 2007. Estimating  
878 denudation from seismic velocities offshore NW Ireland. *Society of Exploration*  
879 *Geophysicists - 77th SEG International Exposition and Annual Meeting, SEG 2007*,  
880 407–411.
- 881 BP 1979. Ireland, Porcupine Basin Well 26/22-1A Geological Completion Report. BP  
882 Petroleum Development Ltd. (Irish Branch), compiled by Dryden, G.J.
- 883 Britoil 1986. Eire Licence 1/82 evaluation of well 35/19-1. Britoil plc, compiled by Harvey, M.  
884 A. & Wild, J. L.
- 885 Brown, A.R. 2001. Calibrate yourself to your data! A vital first step in seismic interpretation.  
886 *Geophysical Prospecting*, **49**, 729–733.
- 887 Brown, A.R. 2011. *Interpretation of Three-Dimensional Seismic Data*. Society of Exploration  
888 Geophysicists & American Association of Petroleum Geologists.
- 889 Chapman, T.J. 1989. The Permian to Cretaceous structural evolution of the Western  
890 Approaches Basin (Melville sub-basin), UK. *Geological Society, London, Special*  
891 *Publications*, **44**, 177–200.
- 892 Chapman, T.J., Broks, T.M., Corcoran, D.V., Duncan, L.A. & Dancer, P.N. 1999. The  
893 structural evolution of the Erris Trough, offshore northwest Ireland, and implications for  
894 hydrocarbon generation. *Petroleum Geology of Northwest Europe: Proceedings of the*  
895 *5th Conference*, 455–469.
- 896 Chew, D.M. & Stillman, C.J. 2009. Late Caledonian orogeny and magmatism. *In: The*  
897 *Geology of Ireland*. 143–173.
- 898 Coleman, A.J., Jackson, C.A.L. & Duffy, O.B. 2017. Balancing sub- and supra-salt strain in  
899 salt-influenced rifts: Implications for extension estimates. *Journal of Structural Geology*,  
900 **102**, 208–225.

- 901 Colin, J.-P., Ioannides, N.S. & Vining, B. 1992. Mesozoic stratigraphy of the Goban Spur,  
902 offshore south-west Ireland. *Marine and Petroleum Geology*, **9**, 527–541.
- 903 Cooper, M.R., Anderson, H., Walsh, J.J., Van Dam, C.L., Young, M.E., Earls, G. & Walker,  
904 A. 2012. Palaeogene Alpine tectonics and Icelandic plume-related magmatism and  
905 deformation in Northern Ireland. *Journal of the Geological Society*, **169**, 29–36.
- 906 Corcoran, D. V & Doré, A.G. 2002. Depressurization of hydrocarbon-bearing reservoirs in  
907 exhumed basin settings: evidence from Atlantic margin and borderland basins.  
908 *Exhumation of the North Atlantic Margin: Timing, Mechanisms and Implications for*  
909 *Petroleum Exploration*, **196**, 457–483.
- 910 Corcoran, D. V & Mecklenburgh, R. 2005. Exhumation of the Corrib Gas Field, Slyne Basin,  
911 offshore Ireland. *Petroleum Geoscience*, **11**, 239–256.
- 912 Corfield, S., Murphy, N. & Parker, S. 1999. The structural and stratigraphic framework of the  
913 Irish Rockall Trough. *Geological Society, London, Petroleum Geology Conference*  
914 *series*, **5**, 407–420.
- 915 Coward, M.P. 1995. Structural and tectonic setting of the Permo-Triassic basins of northwest  
916 Europe. *Geological Society, London, Special Publications*, **91**, 7–39.
- 917 Cunningham, G.A. & Shannon, P.M. 1997. The Erris Ridge: A major geological feature in the  
918 NW Irish Offshore Basins. *Journal of the Geological Society*, **154**, 503–508.
- 919 Croker, P.F. and Shannon, P.M. 1987. The evolution and hydrocarbon prospectivity of the  
920 Porcupine Basin, Offshore Ireland. *Petroleum Geology of Northwest Europe*, **3**, 633–  
921 642.
- 922 Dancer, P.N., Algar, S.T. & Wilson, I.R. 1999. Structural evolution of the Slyne Trough.  
923 *Petroleum Geology of Northwest Europe: Proceedings of the 5th Conference on the*  
924 *Petroleum Geology of Northwest Europe*, **1**, 445–454.
- 925 Dancer, P.N. & Pillar, N.W. 2001. Exploring in the Slyne Basin: a geophysical challenge. *The*  
926 *Petroleum Exploration of Ireland's Offshore Basins*, **188**, 209–222.
- 927 Dancer, P.N., Kenyon-Roberts, S.M., Downey, J.W., Baillie, J.M., Meadows, N.S. & Maguire,  
928 K. 2005. The Corrib gas field, offshore west of Ireland. *Geological Society, London,*  
929 *Petroleum Geology Conference series*, **6**, 1035–1046.
- 930 Deptuck, M.E. & Kendell, K.L. 2017. A Review of Mesozoic-Cenozoic Salt Tectonics Along  
931 the Scotian Margin, Eastern Canada. *In: Permo-Triassic Salt Provinces of Europe,*  
932 *North Africa and the Atlantic Margins*. Elsevier, 287–312.
- 933 Doré, A. 1991. The structural foundation and evolution of Mesozoic seaways between  
934 Europe and the Arctic. *Palaeogeography, Palaeoclimatology, Palaeoecology*, **87**, 441–  
935 492.
- 936 Doré, A.G., Lundin, E.R., Jensen, L.N., Birkeland, O., Eliassen, P.E. & Fichler, C. 1999.  
937 Principal tectonic events in the evolution of the northwest European Atlantic margin.  
938 *Petroleum Geology of Northwest Europe: Proceedings of the 5th Conference*, 41–61.



- 939 Duffy, O.B., Gawthorpe, R.L., Docherty, M. & Brocklehurst, S.H. 2013. Mobile evaporite  
940 controls on the structural style and evolution of rift basins: Danish Central Graben,  
941 North Sea. *Basin Research*, **25**, 310–330.
- 942 Dunford, G.M., Dancer, P.N. & Long, K.D. 2001. Hydrocarbon potential of the Kish Bank  
943 Basin: integration within a regional model for the Greater Irish Sea Basin. *Geological*  
944 *Society, London, Special Publications*, **188**, 135–154.
- 945 Elf 1991. Final Well Report 202/18-1. Elf Enterprise Caledonia Ltd.
- 946 Enterprise 1996a. Well IRE 27/5-1 Geological Completion Report. Enterprise Oil plc,  
947 compiled by Rawlinson, A., Verlander, J., Scotchman, I. & Henderson, G.
- 948 Enterprise 1996b. IRE 18/20-1 Geological Completion Report. Enterprise Oil plc, compiled  
949 by O'Neill, N., Scotchman, I. & Dancer, N.
- 950 Enterprise 2000a. Well IRE 18/25-2 Geological Completion Report. Enterprise Oil plc,  
951 compiled by Pay, M. & Geerlings, P.
- 952 Enterprise 2000b. Well IRE 18/20-3 Geological Completion Report. Enterprise Oil plc,  
953 compiled by Pay, M. & Geerlings, P.
- 954 Enterprise 2000c. Well IRE 18/20-4 Geological Completion Report. Enterprise Oil plc,  
955 compiled by Pay, M. & Geerlings, P.
- 956 Ferrer, O., Jackson, M.P.A., Roca, E. & Rubinat, M. 2012. Evolution of salt structures during  
957 extension and inversion of the Offshore Parentis Basin (Eastern Bay of Biscay).  
958 *Geological Society Special Publication*, **363**, 361–380.
- 959 Franklin, J., Tyrrell, S., Morton, A., Frei, D. & Mark, C. 2019. Triassic sand supply to the  
960 Slyne Basin, offshore western Ireland – new insights from a multi-proxy provenance  
961 approach. *Journal of the Geological Society*, **176**, 1120–1135.
- 962 Fugro. 1994. Field Report Irish Frontier Shallow Coring Project Blocks 19/13 and 27/24 Irish  
963 Sector Atlantic Ocean (Volume I).
- 964 Gardiner, P.R.R. & Visscher, H. 1971. Permian–Triassic Transition Sequence at Kingscourt,  
965 Ireland. *Nature Physical Science*, **229**, 209–210.
- 966 Gardiner, P.R.R. & McArdle, P. 1992. The geological setting of Permian gypsum and  
967 anhydrite deposits in the Kingscourt district, counties Cavan, Meath and Monaghan.  
968 *The Irish minerals industry, 1980 – 1990*, 301-316
- 969 Gerlings, J., Hopper, J.R., Fyhn, M.B.W. & Frandsen, N. 2017. Mesozoic and older rift  
970 basins on the SE Greenland Shelf offshore Ammassalik. *Geological Society Special*  
971 *Publication*, **447**, 375–392.
- 972 Glennie, K.W., 1997. History of exploration in the southern North Sea. *Geological Society,*  
973 *London, Special Publications*, **123**, 5-16.
- 974 Grennan, E. 1992. The Glangevlin gypsum deposit, Co. Cavan. *The Irish minerals*  
975 *industry, 1980 - 1990*, 317-325.

- 976 Hansen, T. H., Clausen, O. R., & Andresen, K. J. (in review) 2020. Thick- and thin-skinned  
977 basin inversion in the Danish Central Graben, North Sea – the role of deep evaporites  
978 and basement kinematics. *Solid Earth Discuss.* <https://doi.org/10.5194/se-2020-127>
- 979 Haughton, P., Praeg, D., Shannon, P., Harrington, G., Higgs, K., Amy, L., Tyrrell, S. &  
980 Morrissey, T. 2005. First results from shallow stratigraphic boreholes on the eastern  
981 flank of the Rockall Basin, offshore western Ireland. *Geological Society, London,*  
982 *Petroleum Geology Conference series*, **6**, 1077–1094.
- 983 Hitchen, K., Stoker, M.S., Evans, D. & Beddoe-Stephens, B. 1995. Permo-Triassic  
984 sedimentary and volcanic rocks in basins to the north and west of Scotland. *Geological*  
985 *Society, London, Special Publications*, **91**, 87–102.
- 986 Hudec, M.R. & Jackson, M.P.A. 2007. Terra infirma: Understanding salt tectonics. *Earth-*  
987 *Science Reviews*, **82**, 1–28.
- 988 Hutton, D.H.W. & Alsop, G.I. 1996. The Caledonian strike-swing and associated lineaments  
989 in NW Ireland and adjacent areas: sedimentation, deformation and igneous intrusion  
990 patterns. *Journal of the Geological Society*, **153**, 345–360.
- 991 Illing, L. V & Griffith, A.E. 1986. Gas Prospects in the ‘Midland Valley’ of Northern Ireland.  
992 *Geological Society, London, Special Publications*, **23**, 73–84.
- 993 Jackson, C.A.L. & Lewis, M.M. 2016. Structural style and evolution of a salt-influenced rift  
994 basin margin; the impact of variations in salt composition and the role of polyphase  
995 extension. *Basin Research*, **28**, 81–102.
- 996 Jackson, C.A.-L. & Stewart, S.A. 2017. Composition, Tectonics, and Hydrocarbon  
997 Significance of Zechstein Supergroup Salt on the United Kingdom and Norwegian  
998 Continental Shelves. *In: Permo-Triassic Salt Provinces of Europe, North Africa and the*  
999 *Atlantic Margins*. Elsevier, 175–201.
- 1000 Jackson, C.A.L., Elliott, G.M., Royce-Rogers, E., Gawthorpe, R.L. & Aas, T.E. 2019. Salt  
1001 thickness and composition influence rift structural style, northern North Sea, offshore  
1002 Norway. *Basin Research*, **31**, 514–538.
- 1003 Jackson, D.I. & Mulholland, P. 1993. Tectonic and stratigraphic aspects of the East Irish Sea  
1004 Basin and adjacent areas: contrasts in their post-Carboniferous structural styles.  
1005 *Geological Society, London, Petroleum Geology Conference series*, **4**, 791–808.
- 1006 Jackson, M.P.A. & Vendeville, B.C. 1994. Regional extension as a geologic trigger for  
1007 diapirism. *Geological Society of America Bulletin*, **106**, 57–73.
- 1008 Jackson, M.P., & Hudec, M.R. 2017a. *Salt tectonics: Principles and practice*. Cambridge  
1009 University Press. 62-75.
- 1010 Jackson, M.P., & Hudec, M.R. 2017b. *Salt tectonics: Principles and practice*. Cambridge  
1011 University Press. 256-303.
- 1012 Jansa, L.F., Bujak, J.P. & Williams, G.L. 1980. Upper Triassic salt deposits of the western  
1013 North Atlantic. *Canadian Journal of Earth Sciences*, **17**, 547–559.

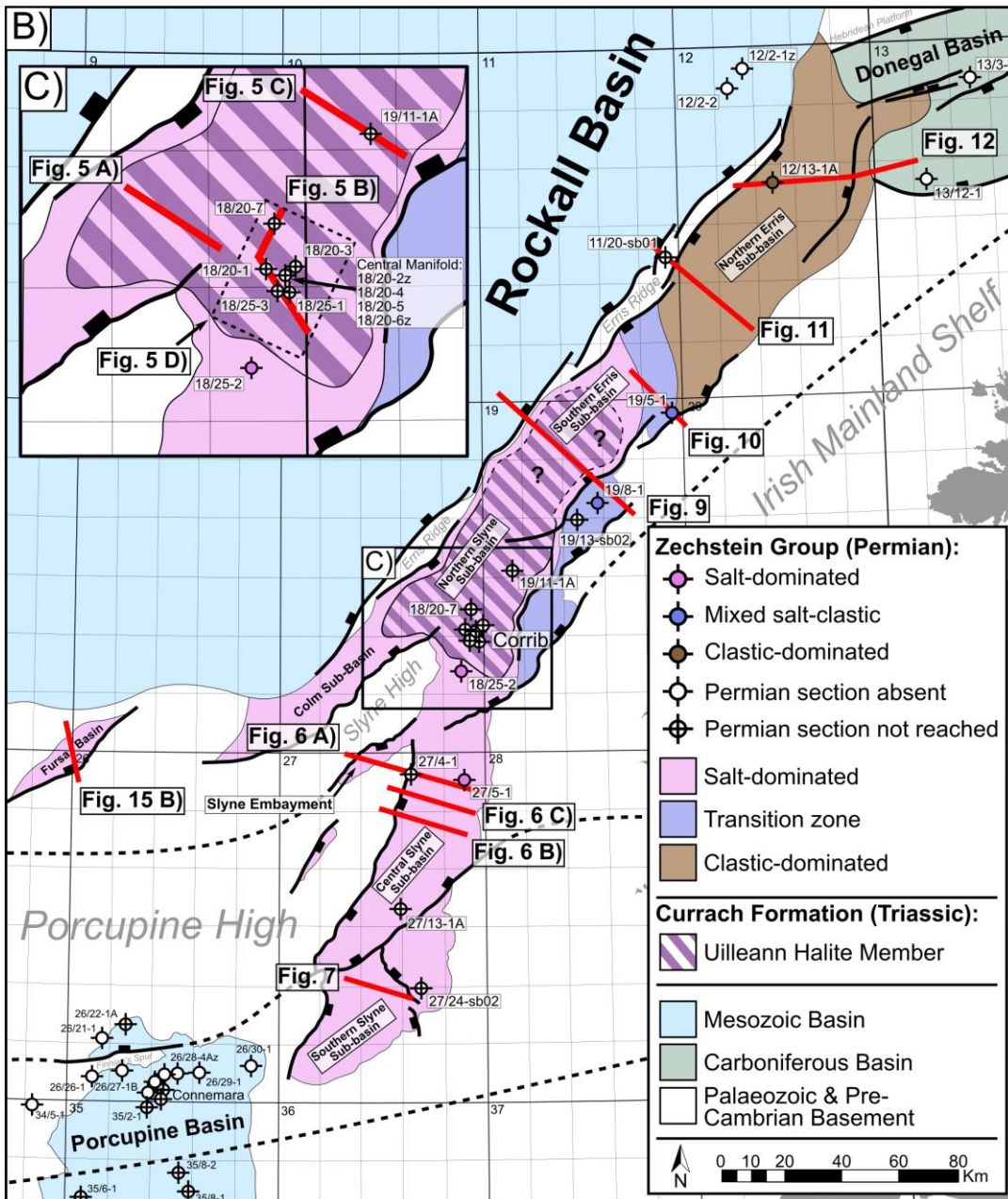
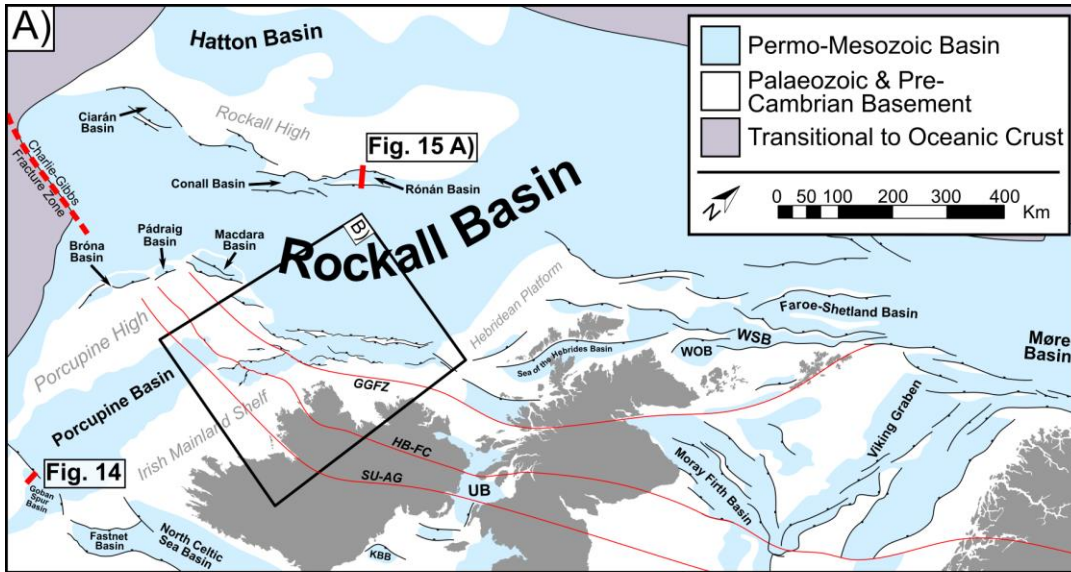
- 1014 Jolley, D.W. & Bell, B.R. 2002. The evolution of the North Atlantic Igneous Province and the  
1015 opening of the NE Atlantic rift. *Geological Society, London, Special Publications*, **197**,  
1016 1–13.
- 1017 Knott, S.D., Burchell, M.T., Jolley, E.J. & Fraser, A.J. 1993. Mesozoic to Cenozoic plate  
1018 reconstructions of the North Atlantic and hydrocarbon plays of the Atlantic margins.  
1019 *Petroleum Geology of Northwest Europe: Proceedings of the 4th Conference*, 953–974.
- 1020 Le Breton, E., Cobbold, P.R. & Zanella, A. 2013. Cenozoic reactivation of the Great Glen  
1021 Fault, Scotland: additional evidence and possible causes. *Journal of the Geological*  
1022 *Society*, **170**, 403–415.
- 1023 Lundin 2006. Well 13/12-1 Inishbeg Prospect End of Well Report. Lundin Britain Ltd.,  
1024 compiled by Craig, D. & Welding, P.
- 1025 McCann, N. 1988. An Assessment of the Subsurface Geology between Magilligan Point and  
1026 Fair Head, Northern Ireland. *Irish Journal of Earth Sciences*, **9**, 71–78.
- 1027 McKie, T. & Shannon, P.M. 2011. Comment on ‘The Permian-Triassic transition and the  
1028 onset of Mesozoic sedimentation at the northwestern peri Tethyan domain scale:  
1029 Palaeogeographic maps and geodynamic implications’ by S. Bourquin, A. Bercovici, J.  
1030 López-Gomez, J. B. Diez, J. Broutin, A. . *Palaeogeography, Palaeoclimatology,*  
1031 *Palaeoecology*, **311**, 136–143.
- 1032 McKie, T. 2017. Paleogeographic Evolution of Latest Permian and Triassic Salt Basins in  
1033 Northwest Europe. *In: Permo-Triassic Salt Provinces of Europe, North Africa and the*  
1034 *Atlantic Margins*. Elsevier, 159–173.
- 1035 Merlin Energy Resources Consortium. 2020. The Standard Stratigraphic Nomenclature of  
1036 Offshore Ireland: An Integrated Lithostratigraphic, Biostratigraphic and Sequence  
1037 Stratigraphic Framework. Project Atlas. Petroleum Affairs Division, Department of the  
1038 Environment, Climate and Communications, Special Publication **1/21**.
- 1039 Naylor, D. & Shannon, P., 1982. Geology of offshore Ireland and west Britain.
- 1040 Naylor, D., Shannon, P.M. and Murphy, N. 1999. *Irish Rockall Basin Region - a Standard*  
1041 *Structural Nomenclature System*. Petroleum Affairs Division, Department of the  
1042 Environment, Climate and Communications, Special Publication **1/99**.
- 1043 Naylor, D. 1992. The post-Variscan history of Ireland. *Geological Society, London, Special*  
1044 *Publications*, **62**, 255–275, <https://doi.org/10.1144/GSL.SP.1992.062.01.21>.
- 1045 Naylor, D., Haughey, N., Clayton, G. & Graham, J.R. 1993. The Kish Bank Basin, offshore  
1046 Ireland. *Petroleum Geology of Northwest Europe: Proceedings of the 4th Conference*,  
1047 **4**, 845–855, <https://doi.org/10.1144/0040845>.
- 1048 Pena dos Reis, R., Pimentel, N., Fainstein, R., Reis, M. & Rasmussen, B. 2017. Influence of  
1049 Salt Diapirism on the Basin Architecture and Hydrocarbon Prospects of the Western  
1050 Iberian Margin. *In: Permo-Triassic Salt Provinces of Europe, North Africa and the*  
1051 *Atlantic Margins*. Elsevier, 313–329.

- 1052 Petroleum Affairs Division. 2005. *Petroleum Systems Analysis of the Slyne, Erris and*  
1053 *Donegal Basins Offshore Ireland - Digital Atlas*. Petroleum Affairs Division, Department  
1054 of the Environment, Climate and Communications, Special Publications **1/05**.
- 1055 Quinn, M.F., Smith, K. & Bulat, J. 2010. A Geological Interpretation of the Nearshore Area  
1056 between Belfast Lough and Cushendun, Northern Ireland, Utilising a Newly Acquired  
1057 2D Seismic Dataset to Explore for Salt Layers for Possible Gas Storage within Man-  
1058 Made Caverns. *British Geological Survey Commissioned Report CR/10/069*.
- 1059 Raine, R., Copestake, P., Simms, M.J. & Boomer, I. 2020. Uppermost Triassic to Lower  
1060 Jurassic sediments of the island of Ireland and its surrounding basins. *Proceedings of*  
1061 *the Geologists' Association*.
- 1062 Ramos, A., Fernández, O., Muñoz, J.A. & Terrinha, P. 2017. Impact of basin structure and  
1063 evaporite distribution on salt tectonics in the Algarve Basin, Southwest Iberian margin.  
1064 *Marine and Petroleum Geology*, **88**, 961–984.
- 1065 Robinson, K.W., Shannon, P.M. & Young, D.G.G. 1981. The Fastnet Basin: An Integrated  
1066 Analysis. In: Illing, L. V. and Hobson, G. D. (eds) *Petroleum Geology of the Continental*  
1067 *Shelf of North-West Europe*.
- 1068 Rojo, L.A., Cardozo, N., Escalona, A. & Koyi, H. 2019. Structural style and evolution of the  
1069 Nordkapp Basin, Norwegian Barents Sea. *AAPG Bulletin*, **103**, 2177–2217.
- 1070 Schiffer, C., Doré, A.G., Foulger, G.R., Franke, D., Geoffroy, L., Gernigon, L., Holdsworth,  
1071 R.E., Kuszniir, N., Lundin, E., McCaffrey, K., Peace, A.L., Petersen, K.D., Phillips, T.B.,  
1072 Stephenson, R., Stoker, M.S. & Welford J.K. 2019. Structural inheritance in the North  
1073 Atlantic. *Earth-Science Reviews*, 102975.
- 1074 Scotchman, I.C., Doré, A.G. & Spencer, A.M. 2018. Petroleum systems and results of  
1075 exploration on the Atlantic margins of the UK, Faroes & Ireland: what have we  
1076 learnt? *Geological Society, London, Petroleum Geology Conference series*, **8**, 187–  
1077 197, <https://doi.org/10.1144/PGC8.14>.
- 1078 Scotese, C.R. & Schettino, A. 2017. Late Permian-Early Jurassic Paleogeography of  
1079 Western Tethys and the World. In: *Permo-Triassic Salt Provinces of Europe, North*  
1080 *Africa and the Atlantic Margins*. Elsevier, 57–95.
- 1081 Shannon, P.M. 1991. Tectonic framework and petroleum potential of the Celtic Sea, Ireland.  
1082 *First Break*, **9**, <https://doi.org/10.3997/1365-2397.1991006>.
- 1083 Shannon, P.M. & Naylor, D. 1998. An assessment of Irish offshore basins and petroleum  
1084 plays. *Journal of Petroleum Geology*, **21**, 125–152.
- 1085 Shell 2009. IRE 12/2-1 West Dooish Exploration Well End of Well Report – Volume 2  
1086 Subsurface Section. Shell E&P Ireland Ltd.
- 1087 Statoil 2004. Well 19/11-1 & 1A Final Well Report. Statoil Exploration (Ireland) Ltd., compiled  
1088 by Hofsøy, R., Skagen, J., Mortensen, H. & Conroy, J.
- 1089 StatoilHydro 2009. Well 19/8-1 Cashel Prospect End of Well Report. Statoil Exploration  
1090 (Ireland) Ltd., compiled by MacTiernan, B., Kleppa, S., Hunnes, O., Sigve-Selnes, K. &  
1091 Igbineweka, O.J.

- 1092 Stewart, S.A., Harvey, M.J., Otto, S.C. & Weston, P.J. 1996. Influence of salt on fault  
1093 geometry: examples from the UK salt basins. *Geological Society, London, Special*  
1094 *Publications*, **100**, 175–202.
- 1095 Stewart, S.A. 2007. Salt tectonics in the North Sea Basin: a structural style template for  
1096 seismic interpreters. *Geological Society, London, Special Publications*, **272**, 361–396.
- 1097 Stoker, M.S., Stewart, M.A., Shannon, P.M., Bjerager, M., Nielsen, T., Blischke, A.,  
1098 Hjelstuen, B.O., Gaina, C., McDermott, K. & Ólavsdóttir, J. 2017. An overview of the  
1099 Upper Palaeozoic–Mesozoic stratigraphy of the NE Atlantic region. *Geological Society,*  
1100 *London, Special Publications*, **447**, 11–68, <https://doi.org/10.1144/SP447.2>.
- 1101 Štolfová, K. & Shannon, P.M. 2009. Permo-Triassic development from Ireland to Norway:  
1102 basin architecture and regional controls. *Geological Journal*, **44**, 652–676.
- 1103 Steel, R.J. & Wilson, A.C. 1975. Sedimentation and tectonism (?Permo-Triassic) on the  
1104 margin of the North Minch Basin. *Journal of the Geological Society*, **131**, 183–200.
- 1105 Swiecicki, T., Wilcockson, P., Canham, A., Whelan, G. & Homann, H. 1995. Dating,  
1106 correlation and stratigraphy of the Triassic sediments in the West Shetlands area.  
1107 *Geological Society Special Publication*, **91**, 57–85.
- 1108 Tate, M.P. & Dobson, M.R. 1989. Late Permian to early Mesozoic rifting and sedimentation  
1109 offshore NW Ireland. *Marine and Petroleum Geology*, **6**, 49–59.
- 1110 Texaco 1978. Well 13/3-1 Final Geological Report. Texaco Ireland Ltd., compiled by Stuart,  
1111 I.A.
- 1112 Thomson, A. & McWilliam, A. 2001. The structural style and evolution of the Bróna Basin.  
1113 *Geological Society, London, Special Publications*, **188**, 401–410.
- 1114 Trueblood, S. and Morton, N. 1991. Comparative Sequence Stratigraphy and Structural  
1115 Styles of the Slyne Trough and Hebrides Basin. *Journal of the Geological Society*, **148**,  
1116 197–201, <https://doi.org/10.1144/gsjgs.148.1.0197>.
- 1117 Trueblood, S. 1992. Petroleum geology of the Slyne Trough and adjacent basins. *Geological*  
1118 *Society Special Publication*, 315–326.
- 1119 Tyrrell, S., Haughton, P.D.W. & Daly, J.S. 2007. Drainage reorganization during breakup of  
1120 Pangea revealed by in-situ Pb isotopic analysis of detrital K-feldspar. *Geology*, **35**,  
1121 971–974.
- 1122 Tyrrell, S., Souders, A.K., Haughton, P.D.W., Daly, J.S. & Shannon, P.M. 2010.  
1123 Sedimentology, sandstone provenance and palaeodrainage on the eastern Rockall  
1124 Basin margin: evidence from the Pb isotopic composition of detrital K-feldspar.  
1125 *Geological Society, London, Petroleum Geology Conference series*, **7**, 937–952.
- 1126 Van Hoorn, B. 1987. The south Celtic Sea/Bristol Channel Basin: origin, deformation and  
1127 inversion history. *Tectonophysics*, **137**, [https://doi.org/10.1016/0040-1951\(87\)90325-8](https://doi.org/10.1016/0040-1951(87)90325-8).
- 1128 Walsh, A., Knag, G., Morris, M., Quinquis, H., Tricker, P., Bird, C. & Bower, S. 1999.  
1129 Petroleum geology of the Irish Rockall Trough – a frontier challenge. *Petroleum*  
1130 *Geology of Northwest Europe: Proceedings of the 5th Conference*, 433–444.

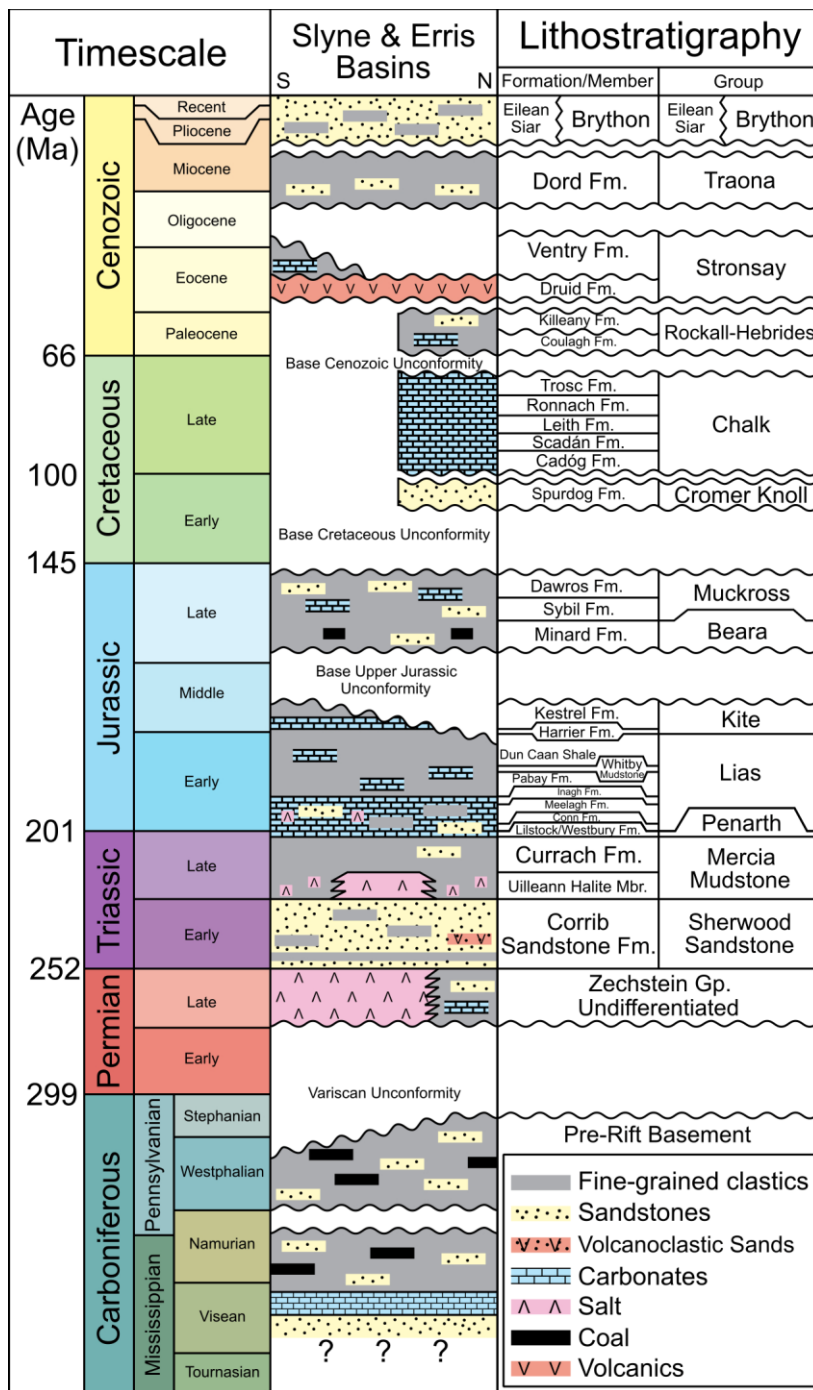
- 1131 Wilson, R.C.L., Hiscott, R.N., Willis, M.G. & Gradstein, F.M. 1989. The Lusitanian Basin of  
1132 west-central Portugal: Mesozoic and Tertiary tectonic, stratigraphic, and subsidence  
1133 history. *Extensional tectonics and stratigraphy of the North Atlantic margins*, 341–361.
- 1134 Withjack, M.O. & Callaway, S. 2000. Active normal faulting beneath a salt layer: An  
1135 experimental study of deformation patterns in the cover sequence. *AAPG Bulletin*, **84**,  
1136 627–651.
- 1137 Zamora, G., Fleming, M. & Gallastegui, J. 2017. Salt Tectonics Within the Offshore Asturian  
1138 Basin. *In: Permo-Triassic Salt Provinces of Europe, North Africa and the Atlantic*  
1139 *Margins*. Elsevier, 353–368.





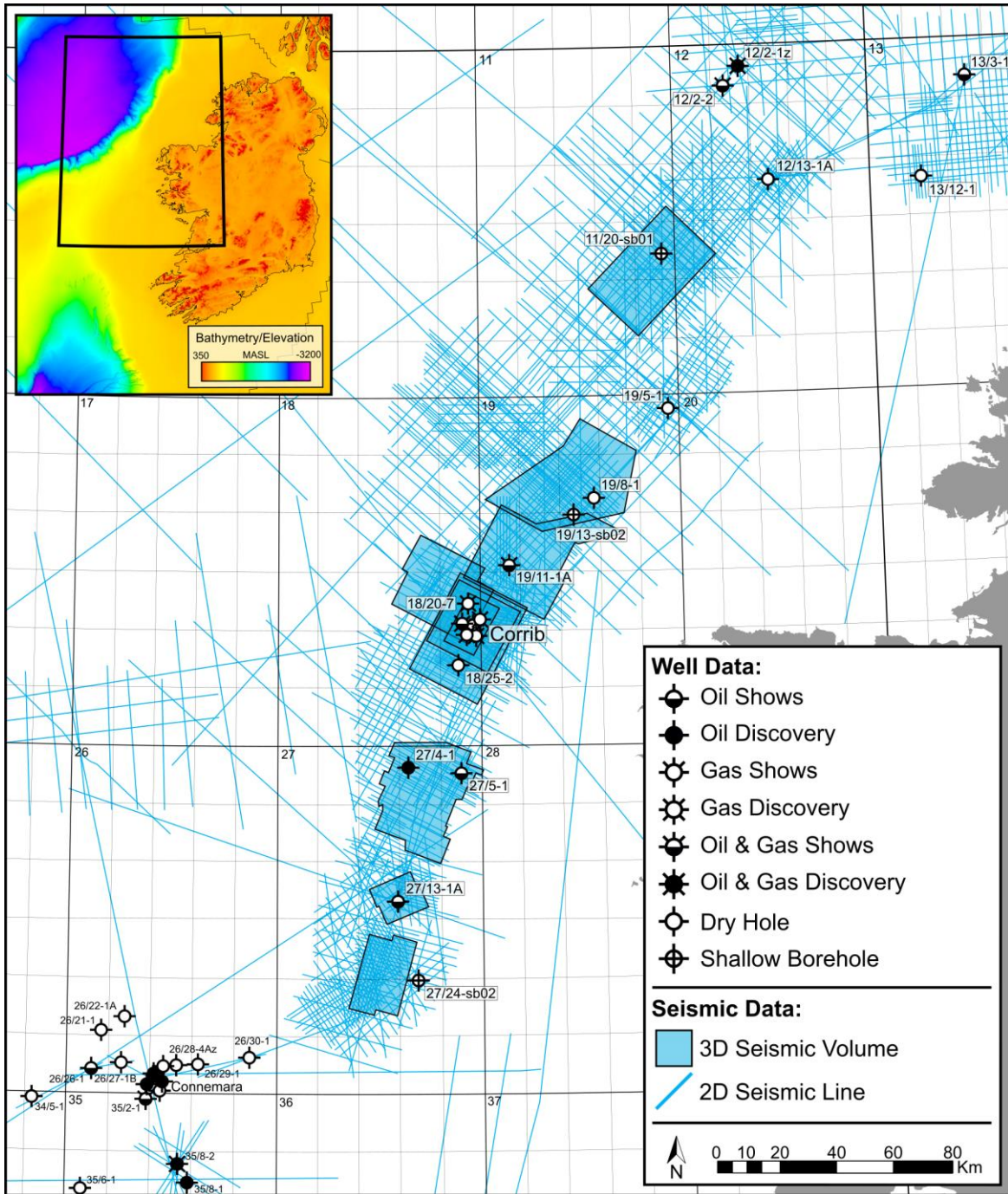


1142 **Figure 1: A)** Map showing the location of the study area and other Permo-Mesozoic basins  
1143 along the north-western European Atlantic margin, adapted from Doré et al. (1999) and Naylor  
1144 et al. (1999). Caledonian structural lineaments which segment the basins are highlighted in  
1145 red. **Abbreviations:** GGFZ – Great Glen Fault Zone; HB-FC – Highland Boundary-Fair Head-  
1146 Clew Bay Lineament; KBB – Kish Bank Basin; SU-AG – Southern Uplands-Antrim-Galway  
1147 Lineament; UB – Ulster Basin; WOB – West Orkney Basin; WSB – West Shetland Basin. **B)**  
1148 Map showing the distribution of Permian and Triassic salt throughout the Slyne and Erris  
1149 basins and neighbouring basins. Faults are displayed at Top Permian offset. **C)** Map showing  
1150 distribution of salt in the Northern Slyne Sub-basin.



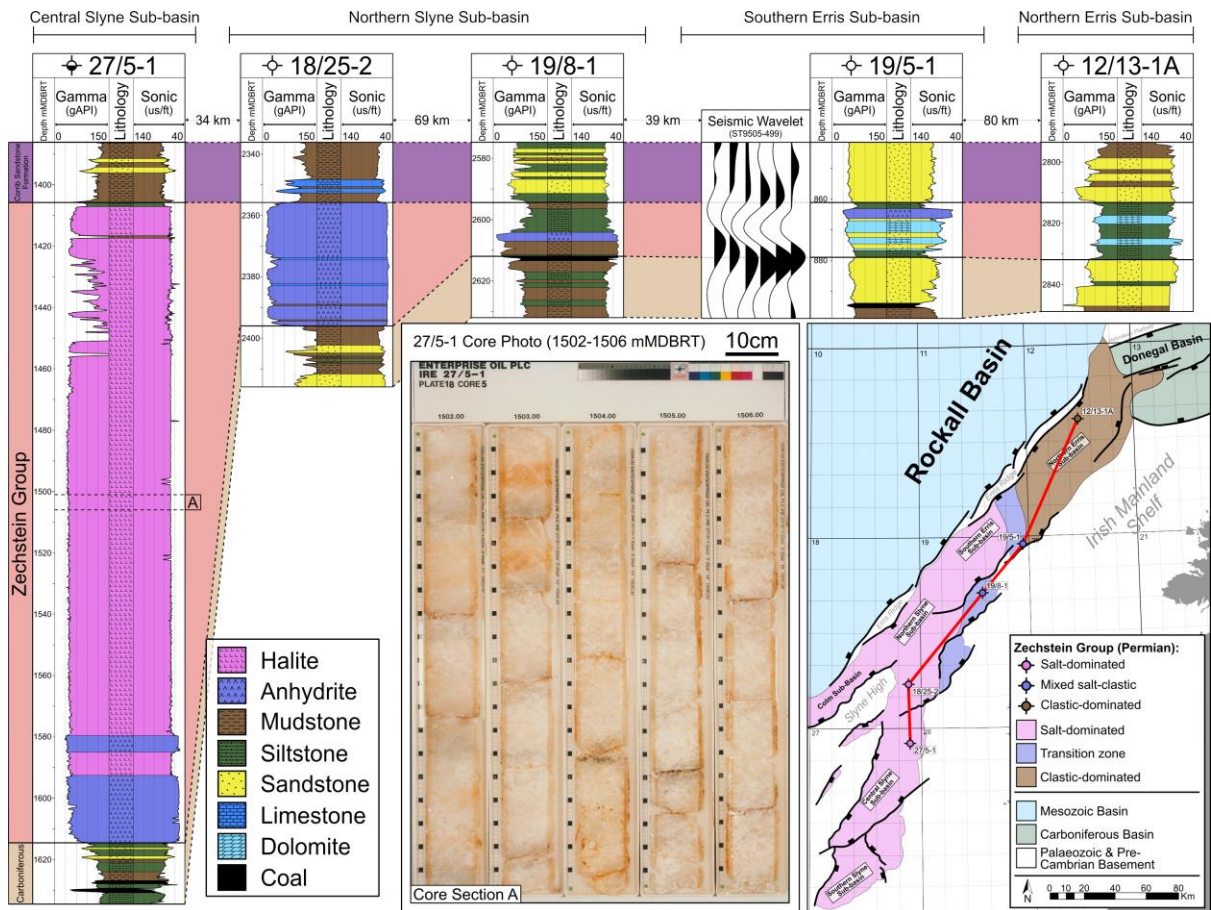
1151

1152 **Figure 2:** Simplified chronostratigraphic chart for the Slyne and Erris basins. Lithostratigraphic  
 1153 nomenclature adapted from Merlin Energy Resources Consortium (2020).



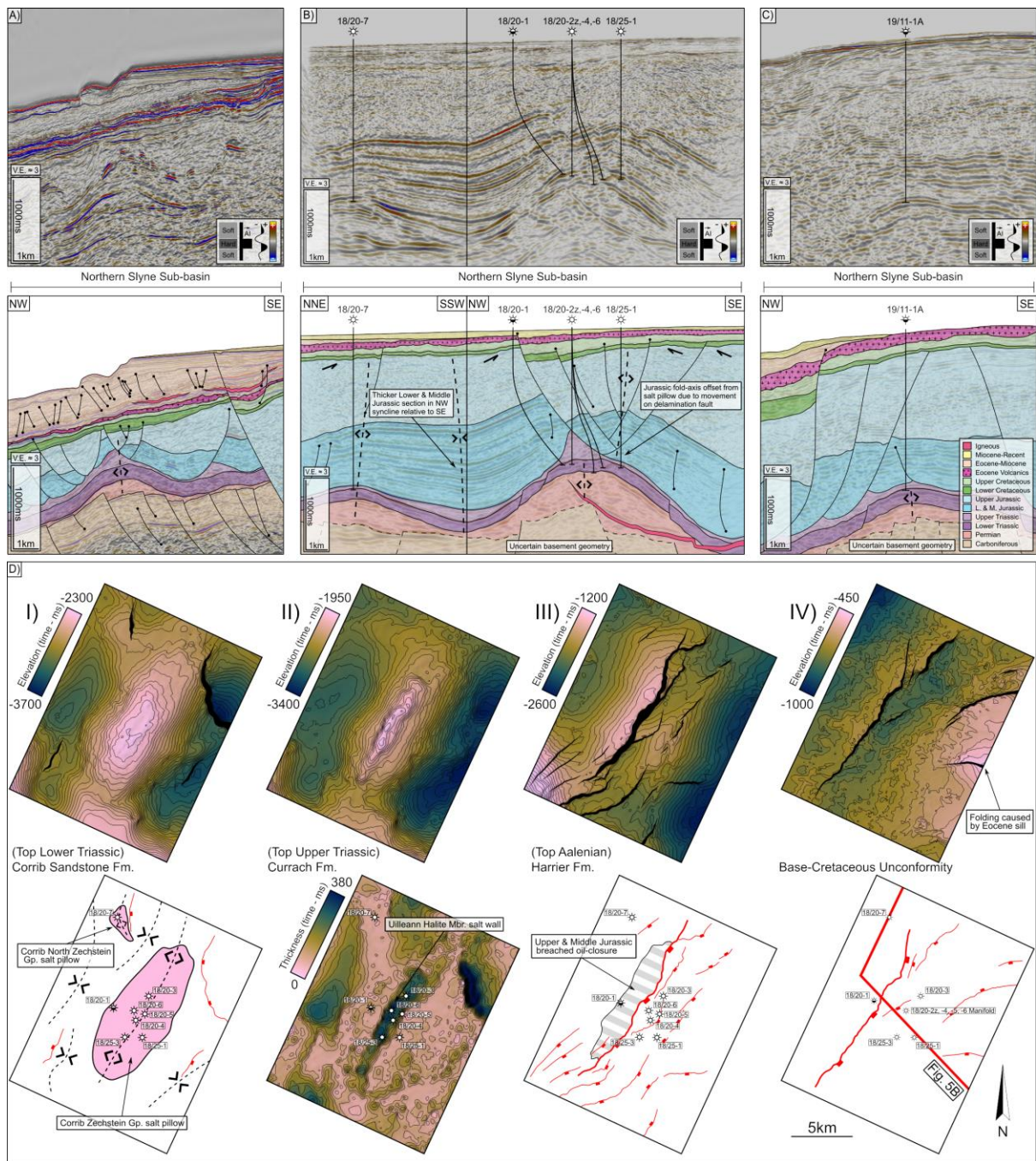
1154

1155 **Figure 3:** Map showing study area and datasets used. **Inset Map:** Bathymetry of the study  
 1156 area.



1157

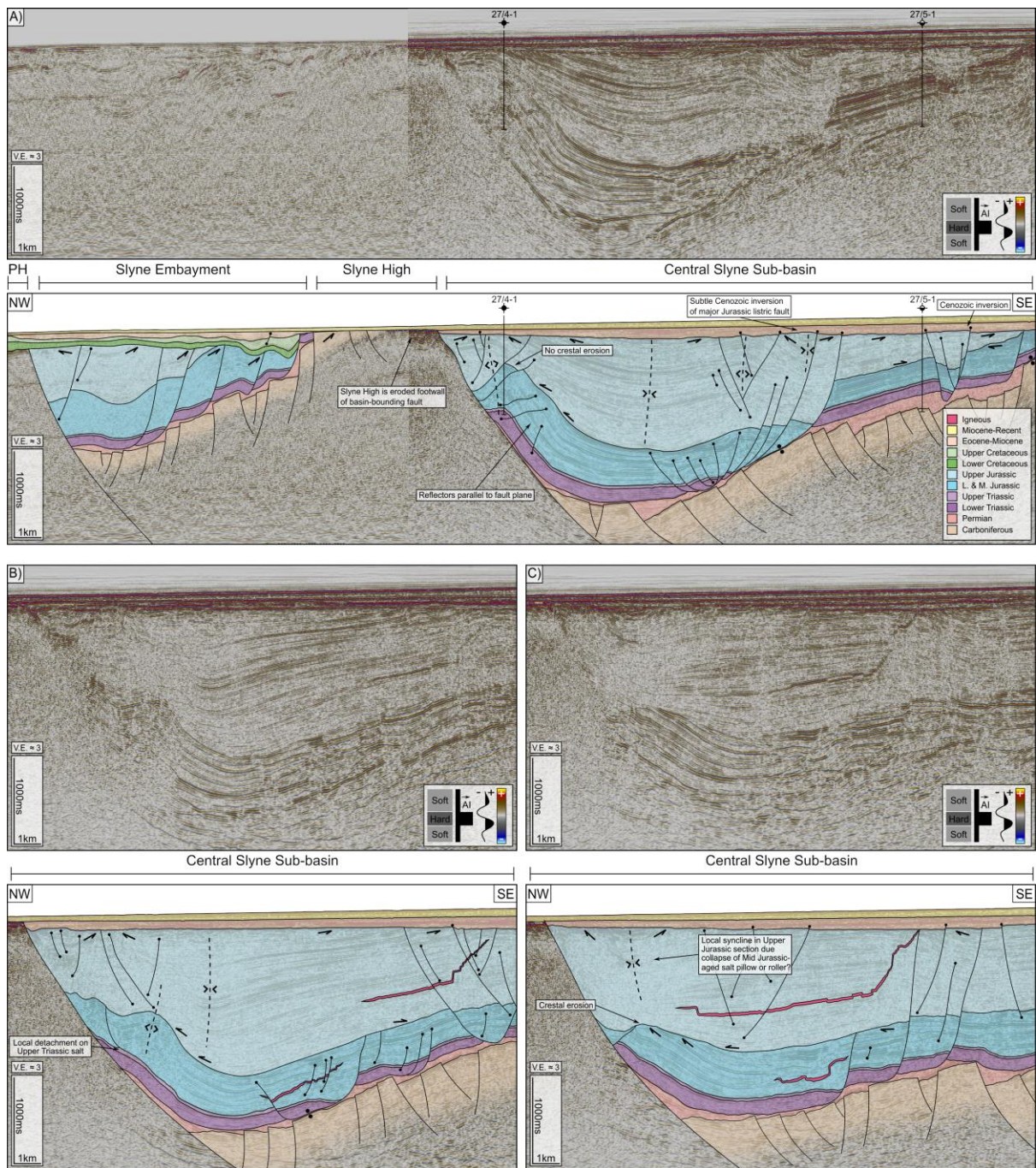
1158 **Figure 4:** Lithological well correlation of the Zechstein Group through the Slyne and Erris  
 1159 basins. Correlation is flattened to the top of the Zechstein Group. **Inset:** Select core photos  
 1160 from the 27/5-1 well in the central Slyne Basin, showing the massive, crystalline, halite-prone  
 1161 Zechstein Group.



1162

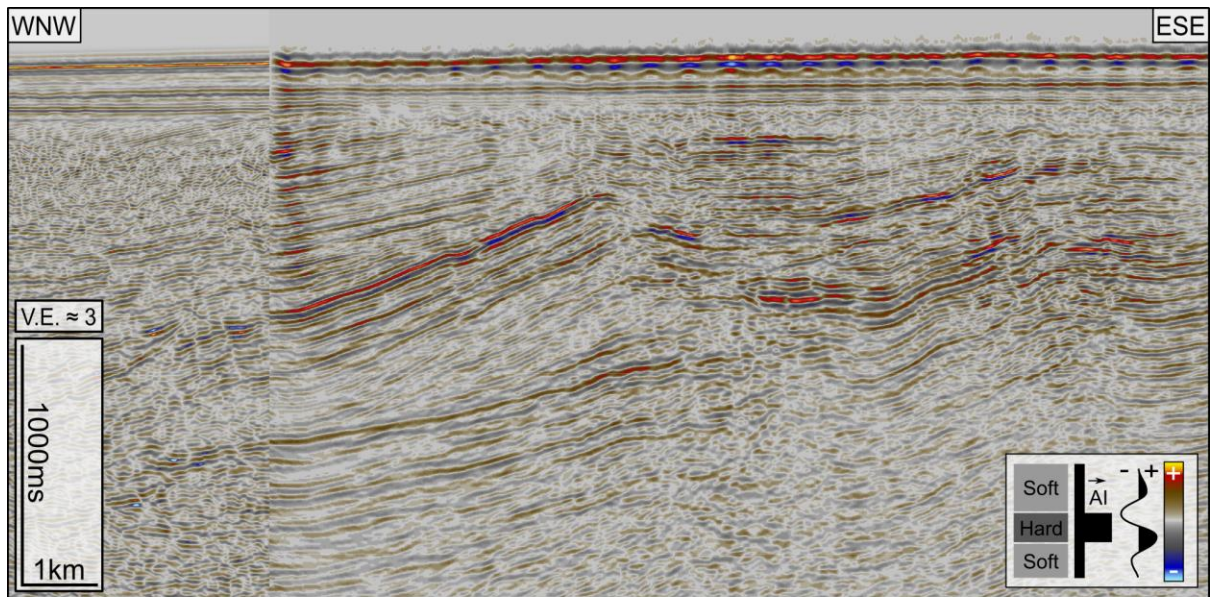
1163 **Figure 5:** Seismic sections from the northern Slyne Basin. See figure 1 for locations. **A)** Inline  
 1164 1600 from the 2018 Inishkea Reprocessed 3D seismic volume and accompanying geoseismic  
 1165 section. A Zechstein Group salt pillow folds the Corrib Sandstone Formation, with delamination  
 1166 faults soling out in the Uilleann Halite Member of the Currach Formation above the crest of  
 1167 the fold. **B)** Arbitrary line from the 2013-01 (13SH3D) 3D seismic volume and accompanying  
 1168 geoseismic interpretation. Two salt-cored folds are visible, one containing the 18/20-7 'Corrib  
 1169 North' gas discovery, and the other containing the Corrib gas field. A major eastward-dipping  
 1170 delamination fault is developed in the Jurassic section above the crest of the Corrib structure,  
 1171 soling out above a small salt diapir within the Uilleann Halite Member, with a faulted rollover

1172 *formed in the hanging-wall of this fault. Well name 18/20-2z, -4, -6 indicates the location of the*  
1173 *subsea manifold for three distinct wells. **C)** Arbitrary line from the 2001/01 3D seismic volume*  
1174 *and accompanying geoseismic section. The salt-cored fold tested by the 19/11-1A well is*  
1175 *shown, with minor delamination faults forming above, soling out in the Uilleann Halite Member*  
1176 *The steep westward dip along the western edge of the structure demonstrates the influence*  
1177 *of post-rift thermal subsidence in the Rockall Basin. **D) I)** Time-structure map of the top Corrib*  
1178 *Sandstone Formation and accompanying map (below) showing Zechstein Group salt pillows.*  
1179 ***II)** Time-structure map of the top Currach Formation and accompanying TWTT thickness map*  
1180 *(below) of the Currach Formation. **III)** Time-structure map of the Top Harrier Formation and*  
1181 *accompanying fault map (below) with the maximum structural closure in the hanging-wall*  
1182 *highlighted (the extent of the residual column encountered in well 18/20-1 is uncertain). **IV)***  
1183 *Time-structure map of the Base-Cretaceous Unconformity and accompanying fault map*  
1184 *(below).*

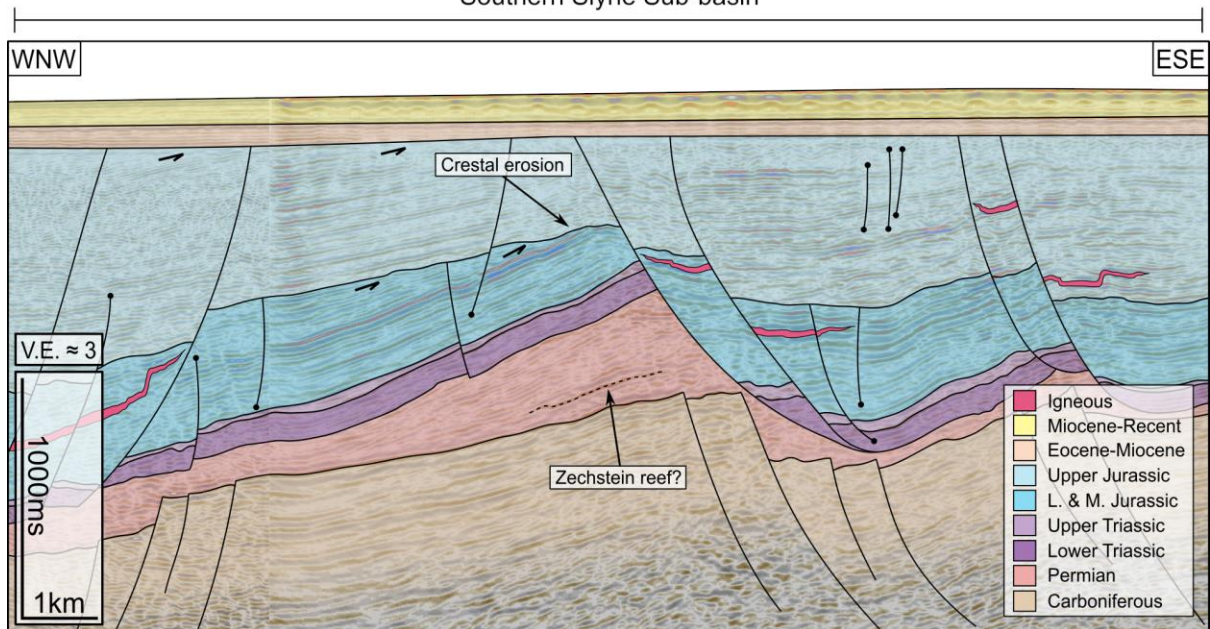


1185

1186 **Figure 6:** Seismic sections from the central Slyne Basin. See figure 1 for seismic line  
 1187 locations. **A)** Composite seismic section of 2D seismic line E96IE09-28 and inline 2740 from  
 1188 the 2000/08 (E00IE09) 3D seismic volume with accompanying seismic interpretation.  
 1189 **Abbreviations:** PH – Porcupine High **B)** Inline 1790 from the 2000/08 (E00IE09) 3D seismic  
 1190 volume with accompanying seismic interpretation. **C)** Inline 2040 from the 2000/08 (E00IE09)  
 1191 3D seismic volume with accompanying seismic interpretation.



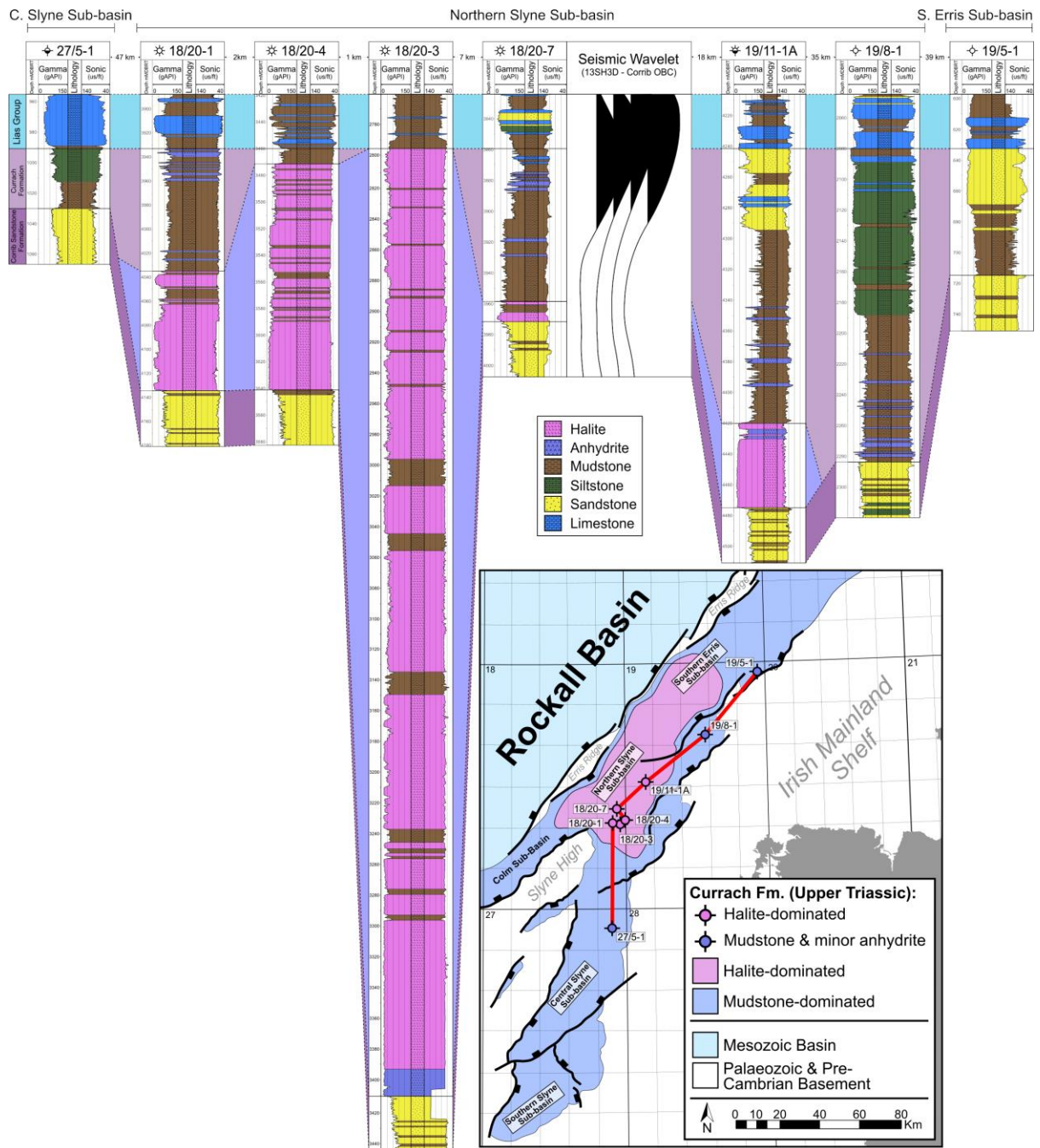
Southern Slyne Sub-basin



1192

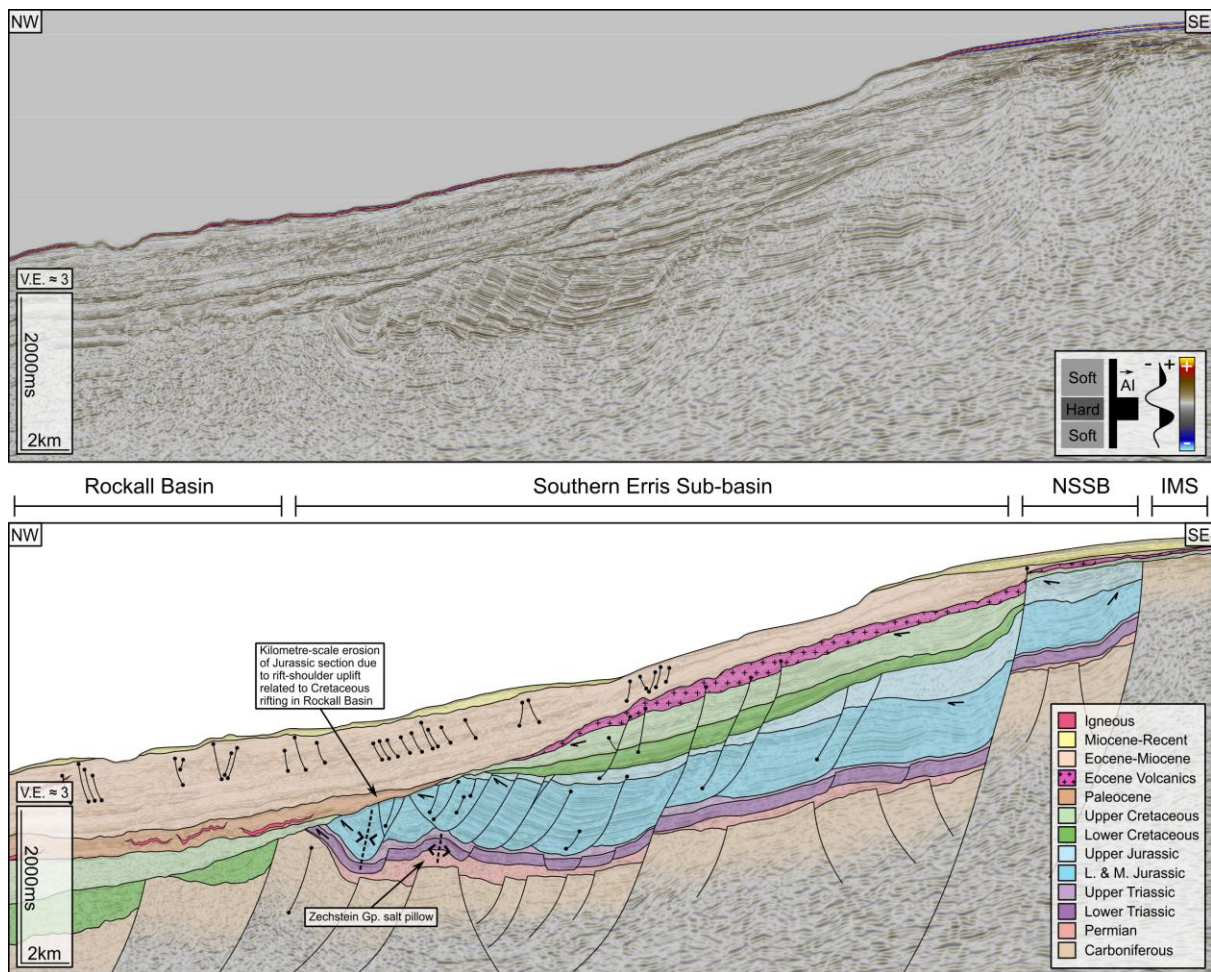
1193 **Figure 7:** Composite seismic section of 2D seismic line TK25-95-32 and crossline 3163 from  
 1194 the 2010/01 (SL103D) 3D seismic volume, with accompanying geoseismic interpretation. The  
 1195 Middle and Lower Jurassic section is severely eroded on the crest of the fault block cored by  
 1196 the large salt roller, with a thicker section preserved in the hanging-wall. See figure 1 for  
 1197 seismic line location.





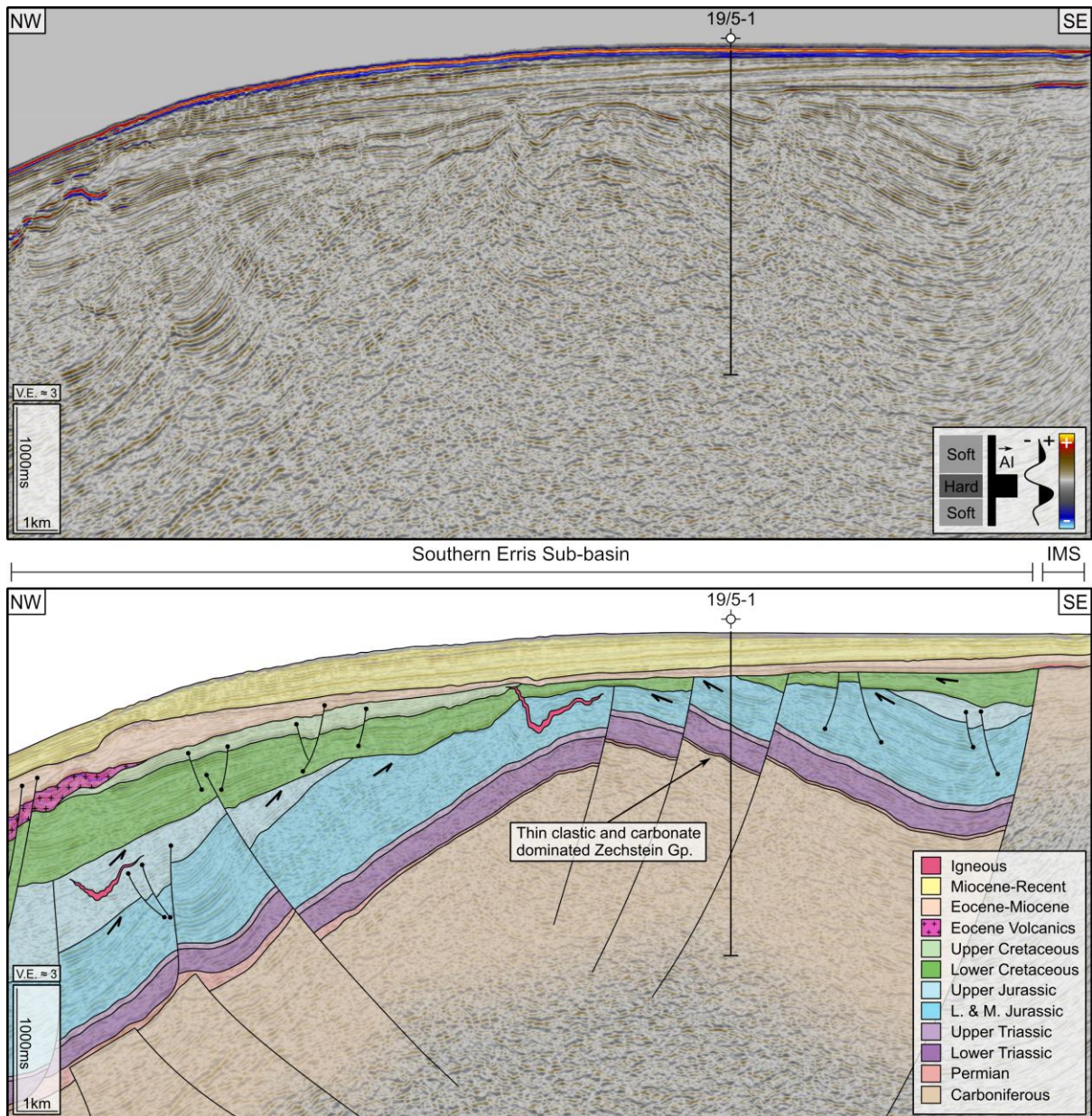
1198

1199 **Figure 8:** Lithological correlation of the Currach Formation and Uilleann Halite Member of  
 1200 select wells through the Slyne and Erris basins. Correlation is flattened to the top of the  
 1201 Currach Formation. Well 18/20-3 penetrates the salt wall above the Corrib salt-cored fold.



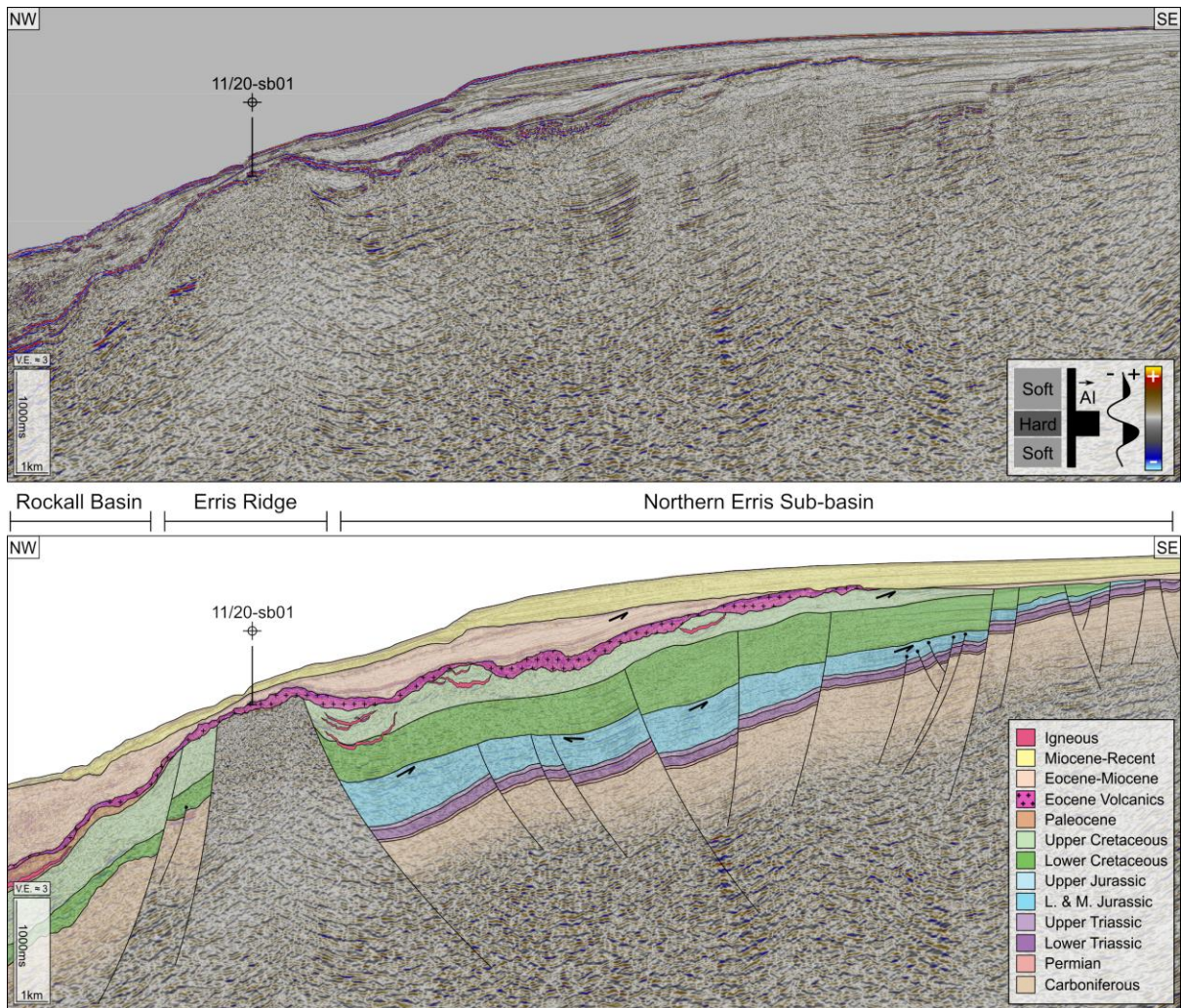
1202

1203 **Figure 9:** 2D seismic line ERM07-6000 and accompanying geoseismic section. The Jurassic  
 1204 section in the southern Erris Basin is dominated by tightly spaced, westward-dipping listric  
 1205 faults which detach on the Uilleann Halite Member. There is also a Zechstein salt pillow  
 1206 evident near the western margin of the basin. Stratigraphy in the Rockall Basin is constrained  
 1207 through correlation with the 12/2-1 and 12/2-2 wells to the NE. See figure 1 for seismic line  
 1208 location. **Abbreviations:** IMS – Irish Mainland Shelf; NSSB – Northern Slyne Sub-basin.



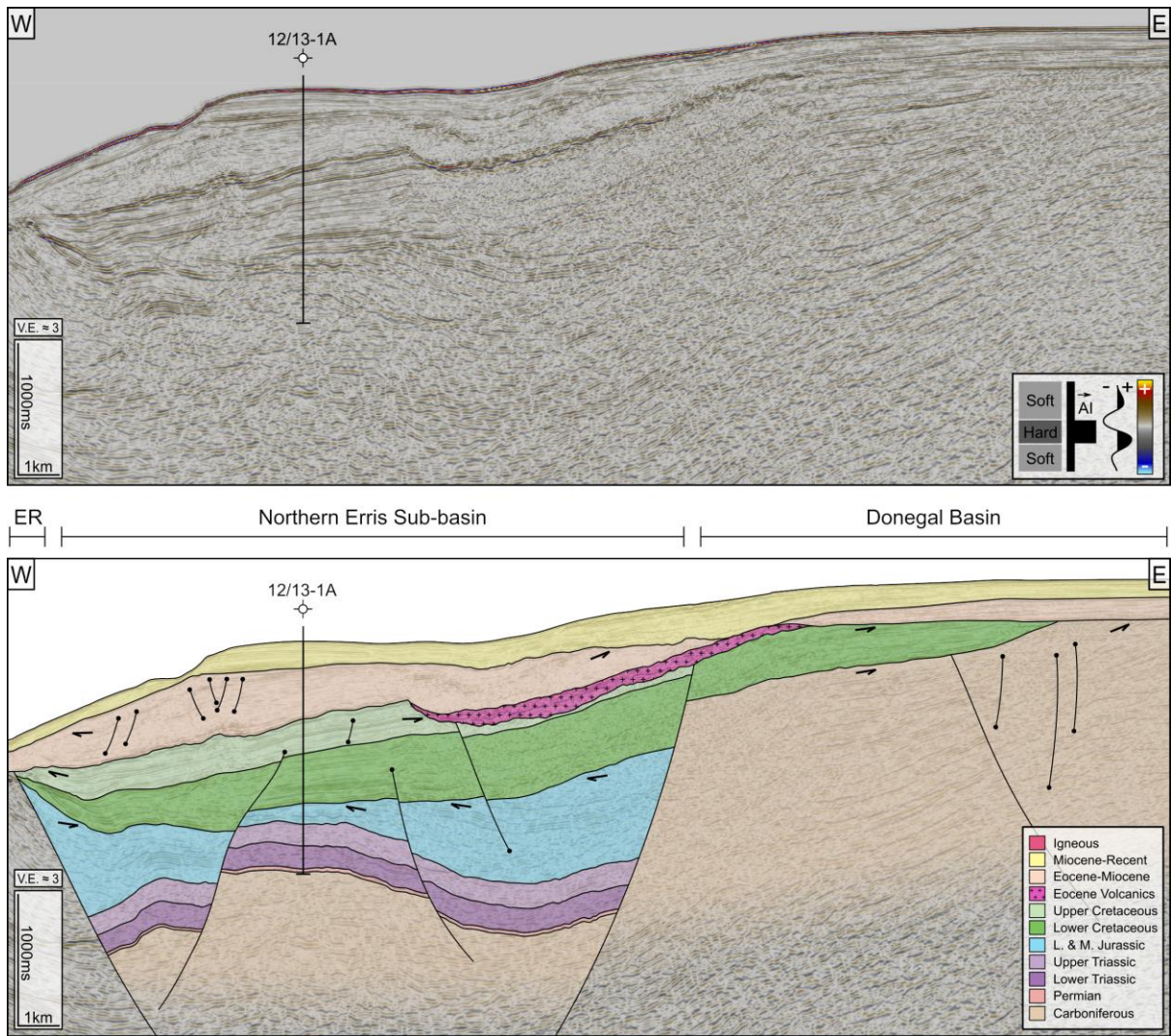
1209

1210 **Figure 10:** 2D seismic line ST9505-449 and accompanying geoseismic section. The  
 1211 proportion of salt in the Zechstein Group increase north-westwards. Faults on the eastern side  
 1212 of the section hard link through the Zechstein Group, while on the western side faults are  
 1213 mechanically detached above and below the Zechstein Group salt. See figure 1 for seismic  
 1214 line location. **Abbreviations:** IMS – Irish Mainland Shelf.



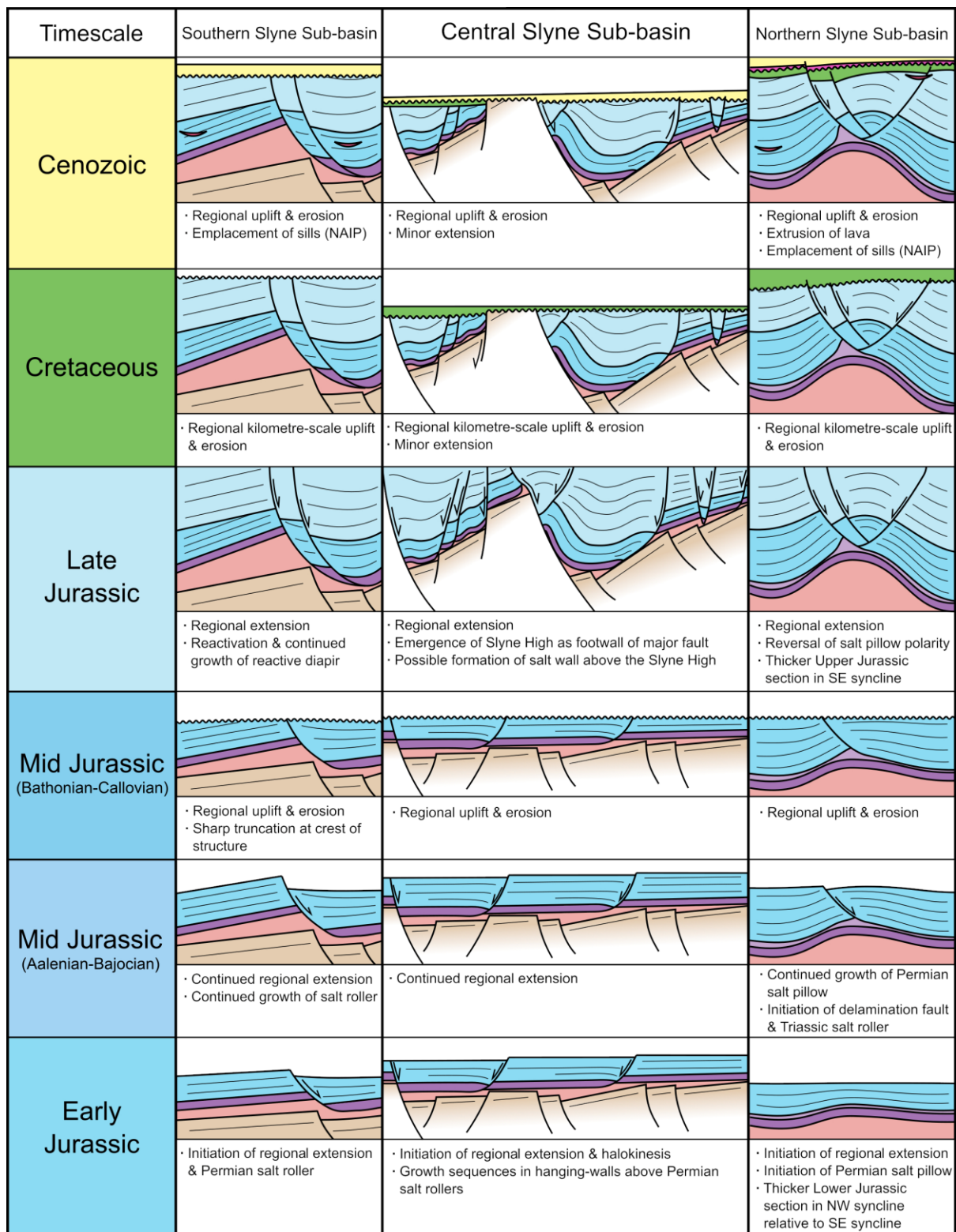
1215

1216 **Figure 11:** 2D seismic line PH98GPO133-027 and accompanying geoseismic section. The  
 1217 northern Erris Basin dips westwards into the bounding fault along the margin of the Erris  
 1218 Ridge, with a significantly reduced Mesozoic section preserved beneath the Base-Cretaceous  
 1219 Unconformity. There is little evidence of salt-related structures in this part of the basin. Eocene  
 1220 lavas cause significant degradation of image quality. See figure 1 for seismic line location.



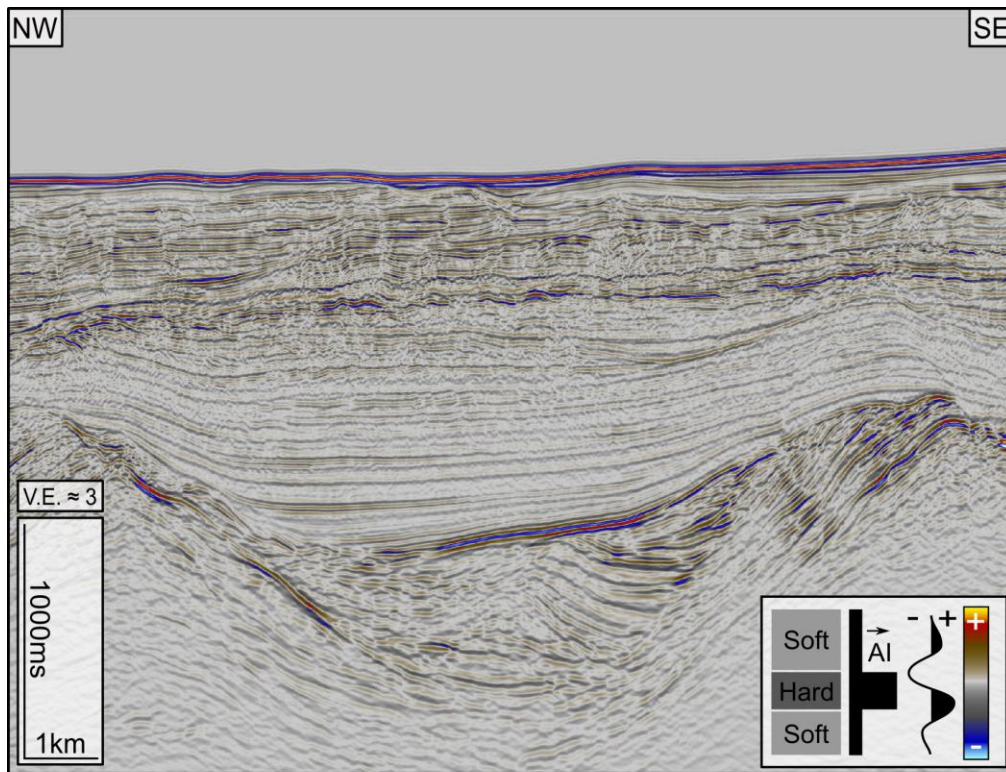
1221

1222 **Figure 12:** 2D seismic line DBS99-304 and accompanying geoseismic section. Here the  
 1223 northern Erris Basin is bounded by the Erris Ridge to the northwest and the Palaeozoic  
 1224 Donegal Basin to the northeast, with a significantly reduced Mesozoic section preserved  
 1225 beneath the BCU. There is little evidence of salt-related structures in this part of the basin.  
 1226 See figure 1 for seismic line location. **Abbreviations:** ER – Erris Ridge.

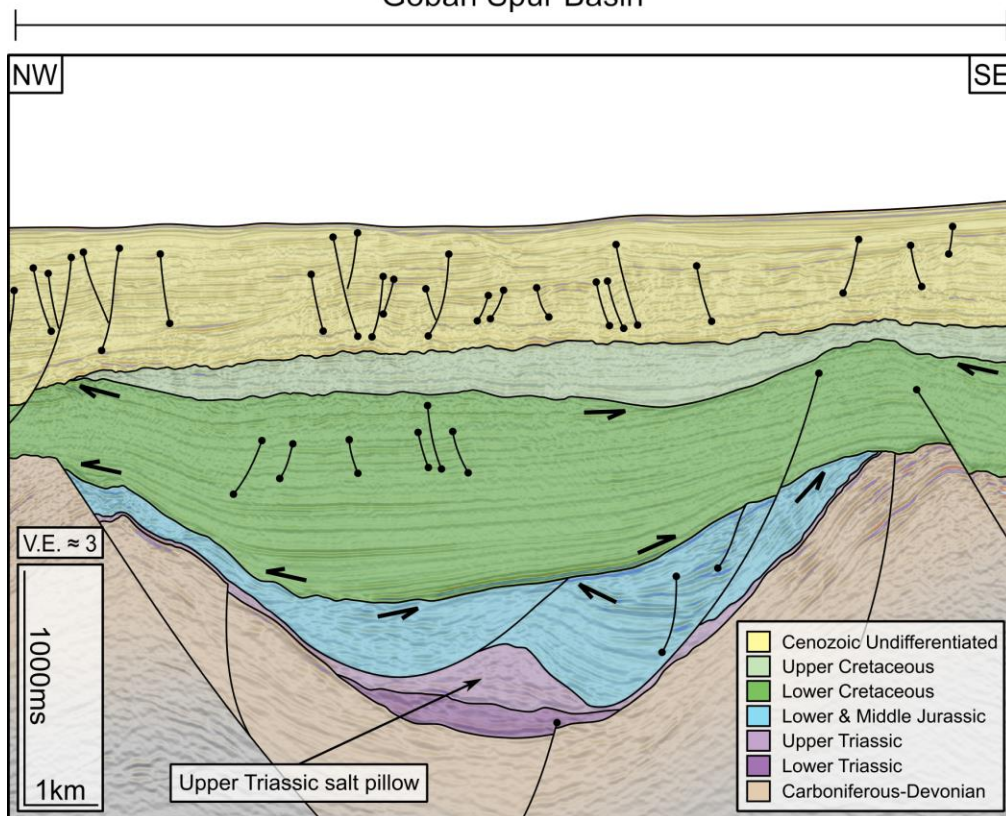


1227

1228 **Figure 13:** Schematic evolutionary model for the formation of different salt-related structures  
 1229 discussed in this study highlighting their multiphase structural evolution. Seismic lines through  
 1230 the structures illustrated in the Southern, Central and Northern Slyne sub-basins are shown  
 1231 in Fig. 6, 7A and 8B respectively. **Abbreviations:** NAIP – North Atlantic Igneous Province.

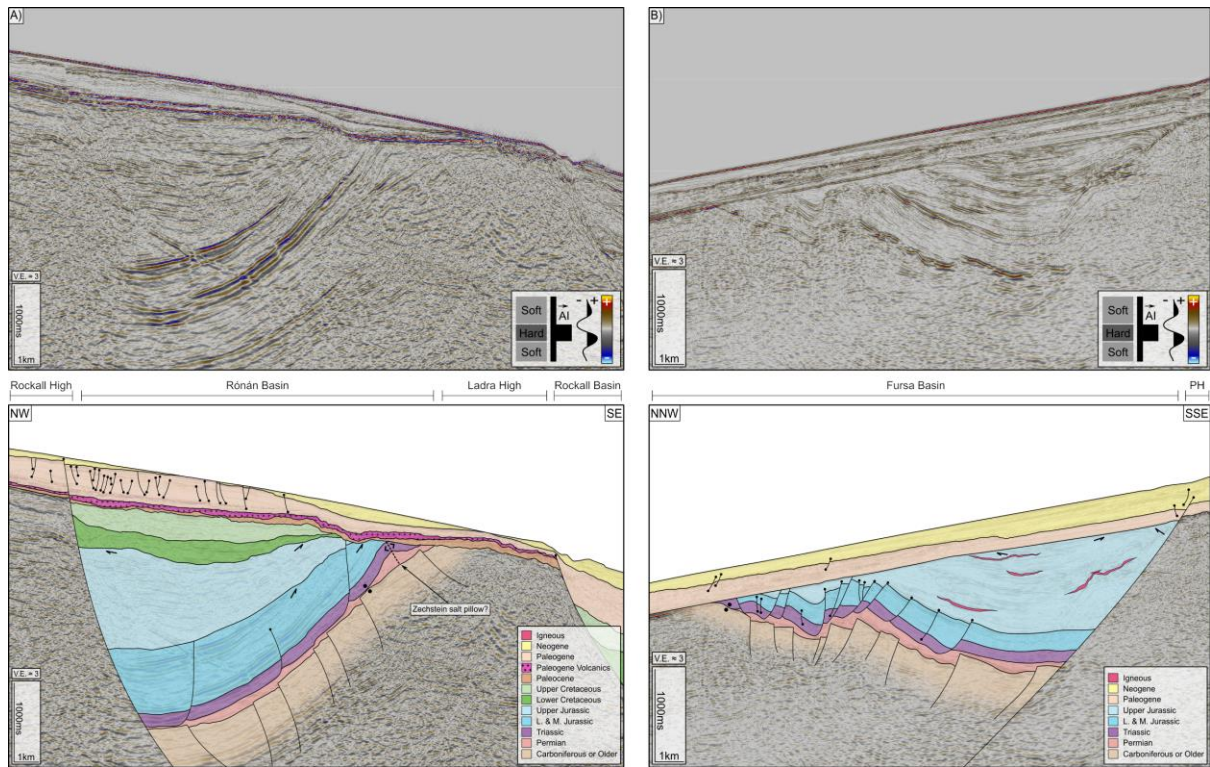


Goban Spur Basin



1232

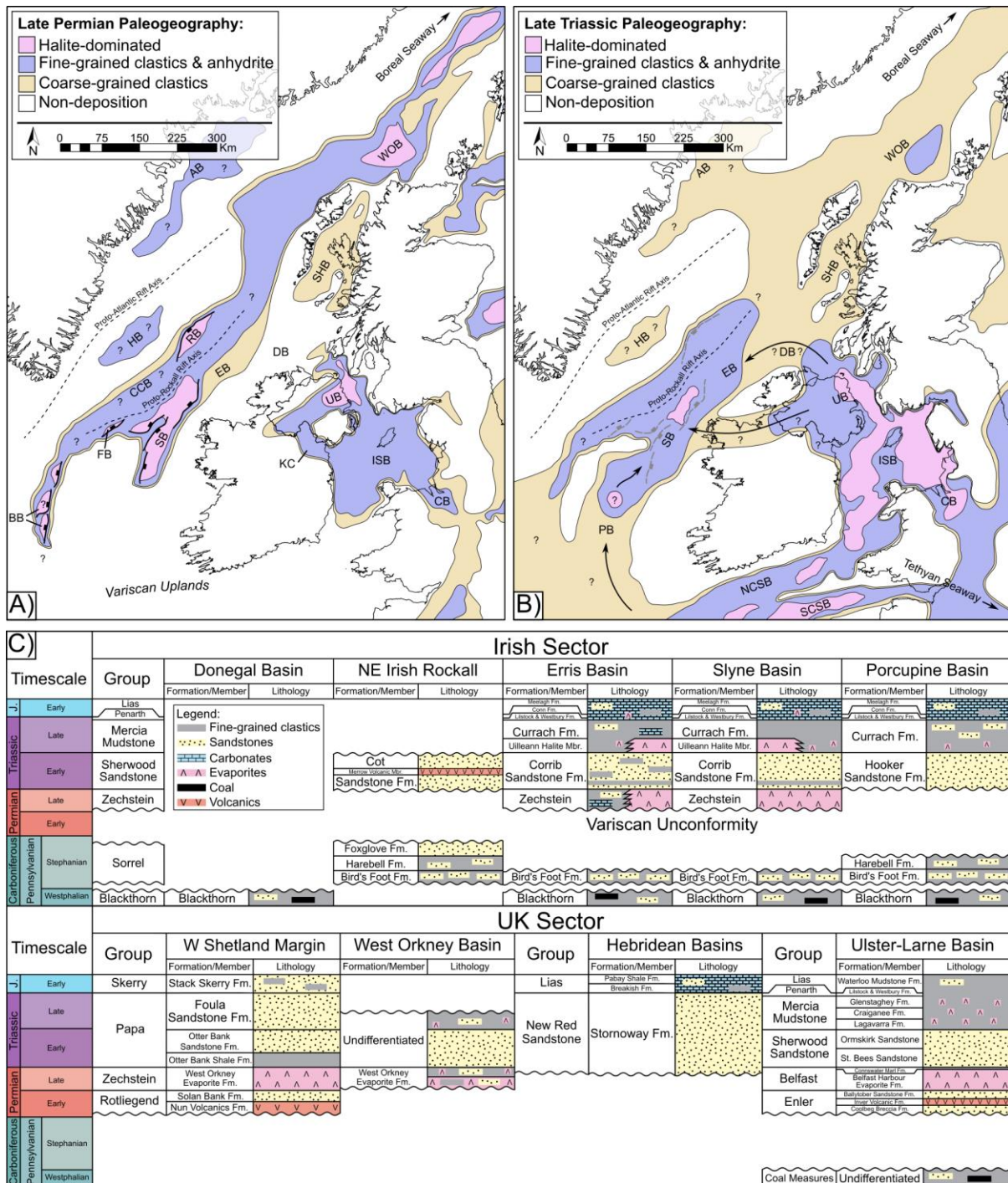
1233 **Figure 14:** Part of 2D seismic line PAD13-044M and accompanying geoseismic section. A  
 1234 distinct décollement surface is observed beneath the Base-Cretaceous Unconformity. An  
 1235 Upper Triassic salt pillow is also observed in this section.



1236

1237 **Figure 15: A)** Part of 2D seismic line WRM96-107 and accompanying geoseismic section.  
 1238 The Rónán Basin is located on the 'conjugate margin' of the Erris Basin on the north-western  
 1239 margin of the Rockall Basin. **B)** Part of 2D seismic line IR11040 and accompanying  
 1240 geoseismic section. A distinct décollement surface is interpreted in the Fursa Basin between  
 1241 the bright top-basement reflector and the overlying Mesozoic section. **Abbreviations:** PH –  
 1242 Porcupine High. **Note:** As the Rónán and Fursa basins are currently undrilled, these  
 1243 interpretations are speculative.





1244

1245 **Figure 16: A)** Schematic Late Permian paleogeographic map of the Irish Atlantic margin and  
 1246 neighbouring regions showing the route of marine ingress from the Boreal Ocean to the Slyne  
 1247 and Erris basins. **B)** Schematic Late Triassic paleogeographic map of the Irish Atlantic margin  
 1248 and neighbouring regions showing three potential routes of marine ingress from the Tethys  
 1249 Ocean to the Slyne and Erris basins. UK sector, Irish Sea and Celtic Sea basins adapted from  
 1250 McKie, 2017. Greenland basins adapted from Gerlings et al., 2017. **C)** Simplified stratigraphic  
 1251 columns of the Upper Pennsylvanian to Lower Jurassic sections from several basins  
 1252 surrounding the study area, showing the broad distribution and composition of Permo-Triassic

1253 rocks. Irish sector adapted from Merlin Energy Resources Consortium (2020), UK sector  
1254 adapted from Stoker et al. (2017), Ulster-Larne Basin adapted from Quinn et al. (2010).  
1255 **Abbreviations:** AB – Ammassalik Basin; BB – Bróna basins; CB – Cheshire Basin; EB – Erris  
1256 Basin; FB – Fursa Basin; HB – Hatton Basin; ISB – Irish Sea basins; KC – Kingscourt; NCSB  
1257 – North Celtic Sea Basin; PB – Porcupine Basin; RB – Rónán Basin; SB – Slyne Basin; SCSB  
1258 – South Celtic Sea Basin; SHB – Sea of the Hebrides Basin; UB – Ulster Basin; WOB – West  
1259 Orkney Basin.